A stoichiometric method for reducing simulation cost of chemical kinetic models

Emmanuel A. Amikiya*and Mapundi K. Banda †

February 21, 2018

Abstract

Mathematical models for chemically reacting systems have high degrees of freedom (very large) and are computationally expensive to analyse. In this discussion, we present and analyse a model reduction method that is based on stoichiometry and mass balances. This method can significantly reduce the high degrees of freedom of such systems. Numerical simulations are undertaken to validate and establish efficiency of the method. A practical example of acid mine drainage is used as a test case to demonstrate the efficacy of the procedure. Analytical results show that the stoichiometrically-reduced model is consistent with the original large model, and numerical simulations demonstrate that the method can accelerate convergence of the numerical schemes in some cases.

Keywords: Chemically reacting systems, mathematical models, model reduction method, numerical simulation, stoichiometry.
MSC: 92E20, 80A30, 92F05

1 Introduction

Acidic mine effluents with high concentrations of corrosive/toxic hydrogen ions, non-metals, dissolved metals metalloids and precipitates pose a major environmental concern. Thus acidic effluents must be treated to reduce or remove the corrosive/toxic species in the waste water. Mathematical models provide quantitative information for understanding the effluent generation and dispersion processes, and also for assessing the impact of the effluents in receiving environments (e.g water quality). This quantitative information enhances the design and implementation of remediation/treatment processes for the effluents [1, 2, 3, 4].

However, such acidic effluents and many other chemical systems are complicated, difficult to model and computationally expensive to simulate. The complications result from the fact that many kinetic systems contain many species that engage in large reaction

*Department of Mathematics and Applied Mathematics, University of Pretoria, Pretoria 0002, South Africa
†Department of Mathematics and Applied Mathematics, University of Pretoria, Pretoria 0002, South Africa

mechanisms at varying time-scales. Thus, mathematical models for such systems are characteristically non-linear, stiff and very large (have high degrees of freedom). While non-linear models that can not be analysed explicitly may be simulated, stiffness issues pose a problem for some numerical procedures [1, 2, 3, 4].

Large models (models with high degrees of freedom) are computationally expensive to simulate. Therefore, methods have been presented in the literature to reduce these systems. Such approaches include: the Steady-State-Approximations (SSA), Partial-Equilibrium-Approximations (PEA) and Asymptotic-Approximations which are based on decoupling [5, 6, 7, 8]. It is also imperative that the reduced models must preserve the essential features of the original large model with significant reduction in computational costs.

The SSA assumes that some species in the system are in quasi-equilibrium, thus differential equations (that describe the evolution of such species) become algebraic equations. Thus the species in quasi-steady state are decoupled from the other species, hence, reducing the model's degrees of freedom. Similarly, the PEA decouples the reactions in the system into fast, medium and slow groups. The fast group is assumed to approach equilibrium and the slow group is discarded, hence, reducing the degrees of freedom of the overall model. These two classes of decoupling approaches require a skillful and knowledgeable chemist to identify the quasi-steady species or fast and slow reactions [5, 6, 7, 8].

Further, sensitivity analysis which involves perturbation of parameters and concentrations, has been performed on some systems to identify fast or slow reactions. In many cases, some researchers report that the approach is successful [5, 9, 10, 11]. However, this approach provides only responses of the original system when the system is subjected to parameter-perturbations, but does not provide enough information about the sensitivity of other closely related systems that contain a common parameter [5, 12, 13, 14].

Other decoupling approaches are the Computational Singular Perturbation (CSP) and the slow manifold methods. The CSP procedure involves analysis of an eigen-decomposition of the original system in order to determine and distinguish fast reactions from slow or dormant reactions [5, 15, 16]. In the slow manifold procedure, a local linearised system is obtained and an analysis of the eigenvalues and eigenvectors is applied to the local linearised system to differentiate the fast reactions from the slow modes in order to obtain a reduced system. This approach is different from other reduction mechanisms because it does not provide single or simple expressions for the chemical kinetics [5, 17, 18, 19, 20].

Furthermore, in a case where non-linear effects cannot be ignored, the methods that are based on linear methodologies can not automatically and sufficiently handle the non-linearities. Thus some global approaches that are capable of handling even non-linearities have also been considered. The challenge with the global approaches is that, when these are employed, they require knowledgeable investigators to monitor the system for possible secondary non-linear effects which can lead to parameter interactions [5, 18].

The stoichiometric method presented and analysed in this discussion maintains key features of the original system and has a remarkable accuracy when applied to chemical kinetic systems. It does not require the detailed input of an expert or specialist apart from the initial modelling process. In this procedure, the species that are of interest to the researcher are decoupled by means of mass balances and stoichiometric ratios. One other advantage of this procedure is that it can be used in conjunction with the procedures

mentioned above to further reduce their degrees of freedom. With this approach, for species under consideration the only data required from the other species, in order to determine the rate profiles of the species of interest, is the set of initial conditions. The reduced model is characteristically nonlinear, stiff and must be positivity preserving. Thus, we will analyse the method by numerical simulation to show its accuracy and efficiency. A practical example from acidic mine effluent treatment will be used as a test case.

The rest of the discussion is organized as follows. A mathematical problem will be formulated in Section 2 and decoupling procedures will be presented in Section 3. Thirdly, we will apply the stoichiometric procedure in Section 4, to acidic effluent kinetics to reduce four and six degrees of freedom to one. Using analytical results, we will also show in Section 4, that the procedure maintains the essential features of the original system. Fourthly, we present in Section 5, numerical schemes (both high and low order consistent) that can resolve stiffness, are positivity-preserving and are conservative. Fifthly, the accuracy and convergence of the numerical schemes will be presented in Sections 6.1. Accuracy and compatibility results for the decoupling methods will be discussed in Section 6.2. Sixthly, we present results for simulation cost in Section 6.3. Finally, we conclude the discussion in Section 7.

2 Chemical kinetic modelling

Chemical kinetics generally involve a **mechanism** (that enumerates all the elementary steps involved in a reaction problem) and **rate data** quantifying the speed with which the reaction proceeds [21, 22, 23]. Mechanisms are described by a set of balanced stoichiometric equations and rate information is quantified by polynomials called rate laws. In this section, we present mathematical models for single and systems of stoichiometric reactions.

2.1 Single reaction mechanism

We begin the discussion here with single stoichiometric reactions and then proceed to systems. The features of reversible reactions also capture those of the irreversible reactions, thus, we consider a hypothetical reversible stoichiometric equation that has N_f species to the left and N_b species to the right (as in Reaction (1) below) making a total of $N = N_f + N_b$ species being involved in the reaction since the species on the left hand of a chemical reaction are distinct from species on the right hand:

$$\sum_{i=1}^{N_f} a_i A_i \rightleftharpoons \sum_{j=1}^{N_b} b_j B_j, \tag{1}$$

where a_i and b_j are stoichiometric coefficients with respect to the species A_i and B_j, respectively.

Denote a vector of all the species in Reaction (1) by $\mathbf{C} = (A_1, A_2, \dots A_{N_f}, B_1, B_2, \dots B_{N_b})$ (i.e left hand side species followed by right hand side species). Let their current concentrations be denoted by $\mathbf{U} = ([A]_1, [A]_2, \dots [A]_{N_f}, [B]_1, [B]_2, \dots [B]_{N_b})$, their orders by $\alpha = (\alpha_1, \alpha_{,2}, \dots \alpha_{N_f}, \beta_1, \beta_2, \dots \beta_{N_b})$, and their stoichiometric coefficients by $\sigma = (a_1, a_2, \dots, a_{N_f},$

$b_1, b_2, \ldots, b_{N_b}$). Then the rate at which the Reaction (1) proceeds can be expressed as follows:

$$R(\mathbf{U}) = K_f \prod_{i=1}^{N_f} U_i^{\alpha_i} - K_b \prod_{j=N_f+1}^{N} U_j^{\alpha_j}, \tag{2}$$

where K_f, K_b are the forward and backward reaction constants, respectively.

Now the rate at which any species C_k (whether left or right of Reaction (1)) evolves can then be expressed as follows:

$$\frac{1}{\sigma_k}\frac{dU_k}{dt} = K_f \prod_{i=1}^{N_f} U_i^{\alpha_i} - K_b \prod_{j=N_f+1}^{N} U_j^{\alpha_j},\ k \in \{1, \ldots, N\}. \tag{3}$$

The right hand side of Equation (3) is a polynomial in N variables (i.e concentrations of all the species). Thus Equation (3) is a system of N ordinary differential equations (ODEs) to be solved simultaneously.

2.2 System of stoichiometric reactions

Let $N_{f,r}$ and $N_{b,r}$ be total species numbers in the forward and backward reactions of an r^{th} elementary reaction, respectively. The mechanism for a system of M elementary reactions involving N species is generally written as:

$$\sum_{i=1}^{N_{f,r}} a_{r,i} A_{r,i} \rightleftharpoons \sum_{j=1}^{N_{b,r}} b_{r,j} B_{r,j}, \quad r = 1, \ldots, M. \tag{4}$$

where $a_{r,i}$ and $b_{r,j}$ are stoichiometric coefficients for the species $A_{r,i}$ and $B_{r,j}$ in the r^{th} elementary reaction, respectively. In general, $\sum_{r=1}^{M}(N_{f,r} + N_{b,r}) \neq N$ due to the presence of networking species (i.e., species engaged in more than one elementary reaction).

Similar to the above discussion, denote

$$\mathbf{C} = (A_1, A_2, \ldots A_N) \text{ and } \mathbf{U} = ([A]_1, [A]_2, \ldots [A]_N),$$

as vectors of all species and their concentrations, respectively. Let a subset of the above species participating in an r^{th} elementary reaction with $N_{f,r}$ and $N_{b,r}$ being the total number of species participating in the reactions on the left and right side, respectively, be denoted as:

$$\begin{aligned} \mathbf{C}_r &= (A_{r,1}, A_{r,2}, \ldots A_{r,N_{f,r}}, B_{r,1}, B_{r,2}, \ldots B_{r,N_{b,r}}) \\ &= (C_{r,1}, C_{r,2}, \ldots C_{r,N_{f,r}}, C_{r,N_{f,r+1}}, C_{r,N_{f,r+2}}, \ldots C_{r,N_r}) \end{aligned}$$

where $N_r = N_{f,r} + N_{b,r}$. Similarly, let

$$\begin{aligned} \mathbf{U}_r &= ([A]_{r,1}, [A]_{r,2}, \ldots [A]_{r,N_{f,r}}, [B]_{r,1}, [B]_{r,2}, \ldots [B]_{r,N_{b,r}}), \\ &= (U_{r,1}, U_{r,2}, \ldots U_{r,N_{f,r}}, U_{r,N_{f,r+1}}, U_{r,N_{f,r+2}}, \ldots U_{r,N_r}) \end{aligned}$$

for $r = 1, 2, \ldots, M$. Further, we define

$$\alpha_r = (\alpha_{r,1}, \alpha_{r,2}, \ldots, \alpha_{r,N_r})$$

as the respective orders of the species in $\mathbf{C}_r$ and

$$\sigma_r = (\sigma_{r,1}, \sigma_{r,2}, \ldots, \sigma_{r,N_r})$$

as their respective stoichiometric coefficients.

The rate at which the r^{th} elementary Reaction (4) proceeds can in general, be expressed as follows:

$$R_r(\mathbf{U}) = K_{fr} \prod_{i=1}^{N_{f,r}} U_{r,i}^{\alpha_{r,i}} - K_{b,r} \prod_{j=N_{f,r}+1}^{N_r} U_{r,j}^{\alpha_{r,j}}, \; r = 1, \ldots, M \tag{5}$$

where $K_{f,r}$, $K_{b,r}$ are the forward and backward reaction constants, respectively. From Equation (5), we obtain the rate at which any species C_k evolves as:

$$\begin{aligned} \frac{dU_k}{dt} &= \sum_{r=1}^{M} \sigma_{kr} R_r, \\ &= \sum_{r=1}^{M} \sigma_{kr} \Big(K_{fr} \prod_{i=1}^{N_{f,r}} U_{r,i}^{\alpha_{r,i}} - K_{b,r} \prod_{j=N_{f,r}+1}^{N_r} U_{r,j}^{\alpha_{r,j}} \Big), \; k = 1, \ldots, N. \end{aligned} \tag{6}$$

Observe in Equation (6) that the right hand side is a polynomial in N variables (i.e concentrations of all the species). Thus Equation (6) is a system of N ordinary differential equations (ODEs) to be solved simultaneously.

However, mechanisms for many reactions are very large (i.e M is large), contain many species (N is large), and corresponding rate law polynomials are very complicated. In many experimental and modelling studies, very few of the species are of interest to the researcher, however, due to networking with other species, the species of interest can not be treated in isolation without first decoupling. In Sections 3, we propose decoupling methods used to surmount such challenges.

3 Model reduction methods

Solving the system of N ordinary differential equations (ODEs) in (3) simultaneously might not be necessary especially if not all the species concentration profiles are required. As an alternative, we propose a decoupling method that will enable only a few species of interest to be solved. In such an approach one can solve for a single species. The single variable rate functions will be functions of current concentration of the species of interest and initial/source data for the other species, as a result, the ODEs will be completely decoupled. For comparison, we also present other decoupling methods that have been used in the literature.

3.1 Stoichiometric decoupling

Denote the initial concentration by $\mathbf{U}_0$, the concentration due to some source/sink by $\mathbf{U}_S$, the transformed concentration by $\mathbf{U}_T$ as the reaction proceeds. Using the concept of mass balance which ensures mass conservation in a given volume (see for example [24, 25] for mass conservation details), we obtain:

$$\mathbf{U} = \mathbf{U}_0 + \mathbf{U}_S + \mathbf{U}_T. \tag{7}$$

In a mass balance expression, transformed concentrations assume positive values if their corresponding species are reaction products and negative otherwise. If the extent of reaction (denoted by χ) is known, then the transformed concentration of a species, is the product of the stoichiometric number and the extent of reaction [22]. This enables us to write the mass balance expressions for any species i, as follows:

$$U_i = U_{0_i} + \sigma_i \chi + U_{S_i}, \quad i = 1, 2, \ldots, N. \tag{8}$$

Assuming that the sources are independent of time, and some algebraic manipulation of Equation (3) using Equation (8) will give:

$$\frac{d\chi}{dt} = K_f \prod_{i=1}^{N_f} \left(U_{0_i} + \sigma_i \chi + U_{S_i}\right)^{\alpha_i} - K_b \prod_{j=N_f+1}^{N} \left(U_{0_j} + \sigma_j \chi + U_{S_j}\right)^{\alpha_j}. \tag{9}$$

Thus χ is the only unknown variable in Equation (9) to be solved for, once χ is known, Equation (8) is used to account for all the species profiles. Depending on how complex Equation (9) is, $\chi(t)$ can be found analytically or numerically, for some rate laws.

In general, if U_{S_k} is time-dependent Equation (8) is re-arranged as follows:

$$\chi = -\frac{1}{\sigma_k}\left(U_{0_k} + U_{S_k}\right) + \frac{1}{\sigma_k} U_k, \; k \in \{1, \ldots, N\}. \tag{10}$$

By substituting Equation (10) into Equation (8), we obtain:

$$\begin{aligned} U_i &= U_{0_i} - \frac{\sigma_i}{\sigma_k}\left(U_{0_k} + U_{S_k}\right) + \frac{\sigma_i}{\sigma_k} U_k + U_{S_i}, \\ &= d_i + \frac{\sigma_i}{\sigma_k} U_k, \; i = 1, 2, \ldots, N, \; k \in \{1, \ldots, N\}, \; k \neq i, \end{aligned} \tag{11}$$

where

$$d_i = U_{0_i} + U_{S_i} - \frac{\sigma_i}{\sigma_k}\left(U_{0_k} + U_{S_k}\right).$$

Applying Equation (11) in the ODE given in Equation (3) for the species of interest, we obtain:

$$\frac{1}{\sigma_k}\frac{dU_k}{dt} = K_f \prod_{i=1}^{N_f} \left(d_i + \frac{\sigma_i}{\sigma_k} U_k\right)^{\alpha_i} - K_b \prod_{j=N_f+1}^{N} \left(d_j + \frac{\sigma_j}{\sigma_k} U_k\right)^{\alpha_j}, \; k \in \{1, \ldots, N\}, \tag{12}$$

whose right hand side is a polynomial of U_k only. Thus for ODE problems that result from a single stoichiometric Reaction (1), one has to solve for one unknown using Equation (12), and then account for the other unknowns using Equation (11).

Furthermore, the stoichiometric procedure can be easily extended to systems of stoichiometric reactions. Similar to the single reaction case, the mass balance expressions for the species in the r^{th} elementary reaction may be written as:

$$U_{r,i} = U_{0_{r,i}} + \sigma_{r,i}\ \chi_r + U_{S_{r,i}},\ i = 1, 2, \ldots, N_r,\ r = 1, \ldots, M \tag{13}$$

where $U_{0_{r,i}}, U_{S_{r,i}}$ are initial data and sources for the i^{th} species in the r^{th} reaction, and χ_r is the extent of reaction. If the species of interest corresponds to the n^{th} element in the subset $\mathbf{U}_r$, then its mass balance expression may be written as:

$$\chi_r = -\frac{1}{\sigma_{r,n}}\Big(U_{0_{r,n}} + U_{S_{r,n}}\Big) + \frac{1}{\sigma_{r,n}}U_{r,n},\ n \in \{1, \ldots, N_r\}. \tag{14}$$

Substituting Equation (14) into Equation (13), we obtain:

$$\begin{aligned} U_{r,i} &= U_{0_{r,i}} - \frac{\sigma_{r,i}}{\sigma_{r,n}}\Big(U_{0_{r,n}} + U_{S_{r,n}}\Big) + \frac{\sigma_{r,i}}{\sigma_{r,n}}U_{r,n} + U_{S_{r,i}}, \\ &= d_{r,i} + \frac{\sigma_{r,i}}{\sigma_{r,n}}U_{r,n},\ i = 1, \ldots, N_r,\ r = 1, \ldots, M,\ n \in \{1, \ldots, N_r\} \end{aligned} \tag{15}$$

where

$$d_{r,i} = U_{0_{r,i}} + U_{S_{r,i}} - \frac{\sigma_{r,i}}{\sigma_{r,n}}\Big(U_{0_{r,n}} + U_{S_{r,n}}\Big).$$

Using Equation (15) in Equation (5), a single-variable rate law for the r^{th} elementary reaction is obtained as follows:

$$R_r = K_{f,r}\prod_{i=1}^{N_{f,r}}\Big(d_{r,i} + \frac{\sigma_{r,i}}{\sigma_{r,n}}U_{r,n}\Big)^{\alpha_{r,i}} - K_{b,r}\prod_{j=1+N_{f,r}}^{N_{r,bf}}\Big(d_{r,j} + \frac{\sigma_{r,j}}{\sigma_{r,n}}U_{r,n}\Big)^{\alpha_{r,j}},\ r = 1, \ldots, M. \tag{16}$$

Moreover, let U_k in the global set $\mathbf{C}$ be the concentration of the species of interest that corresponds to the local concentration $U_{r,n}$ in reaction r. Then the rate at which the species C_k reacts or is produced is given by:

$$\begin{aligned} \frac{dU_k}{dt} &= \sum_{r=1}^{M}\sigma_{kr}R_r, \\ &= \sum_{r=1}^{M}\sigma_{kr}\Big(K_{f,r}\prod_{i=1}^{N_{f,r}}\Big(d_{r,i} + \frac{\sigma_{r,i}}{\sigma_{kr}}U_k\Big)^{\alpha_{r,i}} - K_{b,r}\prod_{j=1+N_{f,r}}^{N_r}\Big(d_{r,j} + \frac{\sigma_{r,j}}{\sigma_{kr}}U_k\Big)^{\alpha_{r,j}}\Big),\ k = 1, \ldots, N, \end{aligned} \tag{17}$$

where $\sigma_{kr} = \sigma_{r,n}$ is the stoichiometric coefficient of the species of interest in the r^{th} elementary reaction. Using vector notation, the decoupled system of species evolution equations may be written as:

$$\frac{d\mathbf{U}}{dt} = S\ \mathbf{R}(\mathbf{U}),\ \mathbf{U}(0) = \mathbf{U}_0,\ t \in [0, T), \tag{18}$$

$\mathbf{U} = (U_1, U_2, \ldots, U_N)^{\mathrm{Tr}}$ is the current concentration vector, $\mathbf{U}_0 = (U_{0_1}, U_{0_2}, \ldots, U_{0_N})^{\mathrm{Tr}}$ is the initial concentration vector, S is an $N \times M$ matrix containing the species stoichiometric values σ_{kr}, $\mathbf{R}(\mathbf{U}) = (R_1, R_2, \ldots, R_M)^{\mathrm{Tr}}$ is a column vector of all the M reaction rate laws and Tr denotes matrix transpose. For a detailed discussion on existence and uniqueness of solutions to the system in (18), see [24, 26].

3.2 Other decoupling methods

The large coupled models in Equation (3) and Equation (6) can also be decoupled by applying Gauss-Seidel, Gauss-Jacobi and Successive-Over-Relaxation (SOR) iterations to the continuous-time models. These methods have been used by the authors in [27] to reduce computational cost.

For convenience of presentation, we rewrite Equation (3) and Equation (6) in the generalized form:

$$\frac{dU_k}{dt} = F_k(\mathbf{U}), \qquad t \in [0, T), \qquad \mathbf{U}(0) = \mathbf{U}_0, \quad k = 1, 2, \ldots, N. \tag{19}$$

The i^{th} continuous-time iteration of system (19) using Gauss-Jacobi iteration is given by:

$$\begin{cases} \frac{d}{dt}U_k^{i+1} = F_k(U_1^i, \ldots, U_{k-1}^i, U_k^{i+1}, U_{k+1}^i, \ldots, U_N^i), \\ \\ U_k^{i+1}(0) = U_{0,i}, \quad k = 1, 2, \ldots, N, \quad t \in [0, T), \quad i = 0, 1, \ldots. \end{cases} \tag{20}$$

Using Gauss-Seidel iteration, the i^{th} continuous-time iteration of (19) states that:

$$\begin{cases} \frac{d}{dt}U_k^{i+1} = F_k(U_1^{i+1}, \ldots, U_{k-1}^{i+1}, U_k^{i+1}, U_{k+1}^i, \ldots, U_N^i), \\ \\ U_k^{i+1}(0) = U_{0,i}, \quad k = 1, 2, \ldots, N, \quad t \in [0, T), \quad i = 0, 1, \ldots. \end{cases} \tag{21}$$

And by using Successive-Over-Relaxation (SOR) iteration, the i^{th} continuous-time iteration (19) states that:

$$\begin{cases} \frac{d}{dt}\bar{U}_k^{i+1} = F_k(U_1^{i+1}, \ldots, U_{k-1}^{i+1}, \bar{U}_k^{i+1}, U_{k+1}^i, \ldots, U_N^i), \\ \\ \bar{U}_k^{i+1}(0) = U_{0,i}, \\ \\ U_k^{i+1} = \omega U_k^i + (1 - \omega)\bar{U}_k^{i+1}, \quad k = 1, 2, \ldots, N, \quad t \in [0, T), \quad i = 0, 1, \ldots, \end{cases} \tag{22}$$

where ω is the relaxation parameter. When $\omega = 0$, the Successive-Over-Relaxation (SOR) reduces to Gauss-Seidel.

4 Acidic effluent generation and treatment models

Acidic mine effluents are water pollutants and environmental hazards that are generated in abandoned mines, and impact adversely on ecological systems upon dispersion. Effluents are composed of an acid and dissolved metals with their precipitates. During treatment of the acidic water, limestone is placed in the acidic water for the calcite in the limestone to neutralize the acid (hydrogen ions). According to [28, 29], three reactions occur simultaneously on the surface of the calcite:

$$CaCO_3 + H^+ \rightleftharpoons Ca^{2+} + HCO_3^-, \tag{23}$$
$$CaCO_3 + H_2CO_3 \rightleftharpoons Ca^{2+} + 2HCO_3^-, \tag{24}$$
$$CaCO_3 + H_2O \rightleftharpoons Ca^{2+} + HCO_3^+ + OH^-, \tag{25}$$

which occur with an overall rate:

$$\begin{aligned} R_{CaCO_3} = {} & K_{H^+}[H^+]^* + K_{H_2CO_3}[H_2CO_3]^* + K_{H_2O}[H_2O]^* \\ & - K_{Ca^{2+}}[Ca^{2+}]^*[H_2CO_3^-]^*, \end{aligned} \tag{26}$$

where $K_{H^+}, K_{H_2CO_3}, K_{H_2O}$ are the forward reaction rate constants in the stoichiometric Equations (23), (24), (25), respectively. The constant $K_{Ca^{2+}}$ is the backward reaction rate constant which depends on temperature and partial pressure of carbon dioxide, P_{CO_2}. The notation $[C]^*$, indicates activity of the chemical species C. Table 1 contains numerical values of the reaction constants.

Table 1: Rate constants for calcite dissolution in units of cm/s given by [28].

K_{H^+}	$K_{H_2CO_3}$	K_{H_2O}	$\log K_{sp}$	$\log K*_{H_2CO_3}$
0.051	$3.45 \times \exp(-5)$	$1.19 \times \exp(-7)$	-8.475	-6.351

The numerical values of the rate constants in Table 1, imply that calcite dissolution by H_2CO_3 and H_2O are far less in comparison to the dissolution by H^+. Thus, in the present discussion, we neglect the sum $K_{H_2CO_3}[H_2CO_3]^* + K_{H_2O}[H_2O]^*$, and express activity of species C, $[C]^*$, in terms of concentration $[C]$ (see, [30, 31, 32] for activity-concentration conversion details). Thus we have;

$$R_{CaCO_3} = F([H^+], [Ca^{2+}], [HCO_3^-]) = K_f[H^+] - K_b[Ca^{2+}][HCO_3^-], \tag{27}$$

$\eta_{HCO_3^-}, \eta_{Ca^{2+}}$ and η_{H^+} are the activity coefficients for HCO_3^-, Ca^{2+} and H^+, respectively, while as $K_f = K_{H^+}\eta_{H^+}$ and $K_b = K_{Ca^{2+}}\eta_{HCO_3^-}\eta_{Ca^{2+}}$. At equilibrium, the rate law in Equation (27) becomes:

$$\begin{aligned} & K_f[H^+] - K_b[Ca^{2+}][HCO_3^-] = 0, \\ & \frac{[Ca^{2+}][HCO_3^-]}{[H^+]} = K_{\text{eq}} \end{aligned} \tag{28}$$

where $K_{\text{eq}} = \frac{K_f}{K_b}$ is the equilibrium constant.

In summary, the dissolution/precipitation reaction of calcite will be described by the stoichiometric Equation (23), and its rate law is Equation (27). From the stoichiometric Equation (23), we have the following data:

$$\mathbf{C} = (CaCO_3,\ H^+,\ Ca^{2+},\ HCO_3^-),\ \mathbf{U} = ([CaCO_3],\ [H^+],\ [Ca^{2+}],\ [HCO_3^-]),\ N_f = 2,\ N = 4,$$
$$\mathbf{U}_0 = ([CaCO_3]_0,\ [H^+]_0,\ [Ca^{2+}]_0,\ [HCO_3^-]_0),\quad \mathbf{U}_S = ([CaCO_3]_S,\ [H^+]_S,\ [Ca^{2+}]_S,\ [HCO_3^-]_S),$$
$$\alpha = (0,\ 1,\ 1,\ 1),\ \text{and}\ \beta = (-1,\ -1,\ 1,\ 1). \tag{29}$$

We make a simplifying assumption here that there are no sources throughout the transient state, so that:

$$[CaCO_3]_S = 0,\quad [H^+]_S = 0,\quad [Ca^{2+}]_S = 0\ \text{ and }\ [HCO_3^-]_S = 0.$$

Substituting data in Equation (29) into (3), with $R = R_{CaCO_3}$ (rate law (27)) the species evolution equations are as follows:

$$-\frac{d[CaCO_3]}{dt} = K_f[H^+] - K_b[Ca^{2+}][HCO_3^-], \tag{30}$$
$$-\frac{d[H^+]}{dt} = K_f[H^+] - K_b[Ca^{2+}][HCO_3^-], \tag{31}$$
$$\frac{d[Ca^{2+}]}{dt} = K_f[H^+] - K_b[Ca^{2+}][HCO_3^-], \tag{32}$$
$$\frac{d[HCO_3^-]}{dt} = K_f[H^+] - K_b[Ca^{2+}][HCO_3^-]. \tag{33}$$

During treatment of the acidic mine effluent water using calcite, one is only interested in knowing whether the concentration of hydrogen ions decreases or not. Thus one only needs to solve Equation (31), in the system of Equations (30) – (33). However, due to coupling with other species the entire set of ordinary differential equations (ODEs (30) – (33)) must be solved simultaneously, which is computationally expensive.

4.1 Stoichiometrically decoupled calcite model

Instead of solving the system (30) – (33) which has four degrees of freedom, we will apply the stoichiometric method (presented in Section 2) to reduce computational cost.

Substituting data (29) into Equation (12) and simplifying, we obtain the stoichiometrically decoupled species evolution equations as follows:

$$-\frac{d[CaCO_3]}{dt} = -K_b[CaCO_3]^2 + \lambda_1[CaCO_3] - \lambda_2, \tag{34}$$
$$-\frac{d[H^+]}{dt} = -K_b[H^+]^2 + \lambda_3[H^+] - \lambda_4, \tag{35}$$
$$\frac{d[Ca^{2+}]}{dt} = \lambda_5 - \lambda_6[Ca^{2+}] - K_b[Ca^{2+}]^2, \tag{36}$$
$$\frac{d[HCO_3^-]}{dt} = \lambda_7 - \lambda_8[HCO_3^-] - K_b[HCO_3^-]^2. \tag{37}$$

where

$$[CaCO_3]_H = [H^+]_0 - [CaCO_3]_0,\ [CaCO_3]_C = [H^+]_0 + [CaCO_3]_0,\ [CaCO_3]_{HC} = [H^+]_0 + [CaCO_3]_0,$$
$$\lambda_1 = K_f + K_b\Big([CaCO_3]_C + [CaCO_3]_{HC}\Big),\ \lambda_2 = K_f[CaCO_3]_H - K_b\Big([CaCO_3]_C + [CaCO_3]_{HC}\Big)$$
$$\lambda_3 = K_f + K_b\Big([H^+]_0 + [HCO_3^-]_0\Big) + K_b\Big([H^+]_0 + [Ca^{2+}]_0\Big),\ \lambda_4 = K_b\Big([H^+]_0 + [HCO_3^-]_0\Big)\Big([H^+]_0$$
$$+ [Ca^{2+}]_0\Big),\ \ \lambda_5 = K_f\Big([H^+]_0 + [Ca^{2+}]_0\Big),\ \lambda_6 = \Big(K_f + K_b[H^+]_0 - K_b[Ca^{2+}]_0,\Big)$$
$$\lambda_7 = K_f\Big([H^+]_0 + [HCO_3^-]_0\Big),\ \lambda_8 = \Big(K_f + K_b[H^+]_0 - K_b[HCO_3^-]_0\Big).$$

By observation, one can easily verify that the ODEs (34)-(37) are completely uncoupled and may be analysed/solved individually at a less cost (see Section 6.3).

4.2 Stoichiometrically decoupled pyrite oxidation model

Exposure and subsequent oxidation of pyrite (and most sulphur-containing minerals) leads to the generation of acids. Such minerals are exposed to air and water in large quantities during mining processes. The stoichiometry of the oxidation include [32, 35, 36]:

$$FeS_2 + 3.5O_2 + H_2O \longrightarrow Fe^{2+} + 2SO_4^{2-} + 4H^+, \tag{38}$$
$$Fe^{2+} + H^+ + 0.25O_2 \longrightarrow Fe^{3+} + 0.5H_2O, \tag{39}$$
$$FeS_2 + 14Fe^{3+} + 8H_2O \longrightarrow 15Fe^{2+} + 2SO_4^{2-} + 16H^+. \tag{40}$$

The rate laws are taken as follows:

$$R_{O_2} = K_{f1}[FeS_2][O_2] - K_{b1}[Fe^{2+}][H^+][SO_4^{2-}], \tag{41}$$
$$R_{Fe^{3+}} = K_{f2}[FeS_2][Fe^{3+}] - K_{b2}[Fe^{2+}][H^+][SO_4^{2-}], \tag{42}$$
$$R_{Fe^{2+}} = K_{f3}[O_2][Fe^{2+}]. \tag{43}$$

The species evolution model is given by:

$$\frac{d\mathbf{U}}{dt} = \mathbf{F}, \tag{44}$$

where $\mathbf{U} = \big([H^+], [FeS_2], [O_2], [Fe^{2+}], [SO_4^{2-}], [Fe^{3+}]\big)^{\text{Tr}}$ and $\mathbf{F} = \big(2R_{O_2} + 16R_{Fe^{3+}} - R_{Fe^{2+}},\ \ -R_{O_2} - R_{Fe^{3+}},\ \ -3.5R_{O_2} - 0.25R_{Fe^{2+}},\ \ R_{O_2} + 15R_{Fe^{3+}} - R_{Fe^{2+}},\ \ 2R_{O_2} + 2R_{Fe^{3+}},\ \ -14R_{Fe^{3+}} + R_{Fe^{2+}}\big)^{\text{Tr}}$.

One can observe coupling in System (44), which implies that the entire set of ODEs (44) must be solved simultaneously. To avoid solving the entire System (44), we apply stoichiometric decoupling on the hydrogen equation in System (44), (with initial and source vectors given by $\mathbf{U}_0 = \big([H^+]_0, [FeS_2]_0, [O_2]_0, [Fe^{2+}]_0, [SO_4^{2-}]_0, [Fe^{3+}]_0\big)^{\text{Tr}}$ and $\mathbf{U}_S = \big([H^+]_S, [FeS_2]_S, [O_2]_S, [Fe^{2+}]_S, [SO_4^{2-}]_S, [Fe^{3+}]_S\big)^{\text{Tr}}$, respectively) to yield:

$$\frac{d[H^+]}{dt} = D_1 + D_2[H^+] + D_3[H^+]^2 + D_4[H^+]^3, \tag{45}$$

where

$$C_{20S} = [FeS_2]_0 + [FeS_2]_S + 0.5([H^+]_0 + [H^+]_S),\ C_{30S} = [O_2]_0 + [O_2]_S + \frac{7}{4}([H^+]_0 + [H^+]_S),$$
$$C_{40S} = [Fe^{2+}]_0 + [Fe^{2+}]_S - 0.5([H^+]_0 + [H^+]_S),\ C_{50S} = [SO_4^{2-}]_0 + [SO_4^{2-}]_S - ([H^+]_0 + [H^+]_S),$$
$$C_{202S} = [FeS_2]_0 + [FeS_2]_S + \frac{1}{16}([H^+]_0 + [H^+]_S),\ C_{404S} = [Fe^{2+}]_0 + [Fe^{2+}]_S - \frac{15}{16}([H^+]_0 + [H^+]_S),$$
$$C_{505S} = [SO_4^{2-}]_0 + [SO_4^{2-}]_S - \frac{2}{16}([H^+]_0 + [H^+]_S),\ C_{606S} = [[Fe^{3+}]_0 + [[Fe^{3+}]_S + \frac{14}{16}([H^+]_0 + [H^+]_S),$$
$$C_{03S} = [O_2]_0 + [O_2]_S - 0.25([H^+]_0 + [H^+]_S),\ C_{04S} = [Fe^{2+}]_0 + [Fe^{2+}]_S - ([H^+]_0 + [H^+]_S),$$

$$D_1 = 2.9K_{f1}C_{20S}C_{30S} + 23.2K_{f2}C_{202S}C_{606S} - 1.45K_{f3}C_{04S}C_{03S}$$
$$D_2 = -K_{f1}\Big(\frac{7}{2}C_{20S} + C_{30S}\Big) - 2K_{b1}C_{40S}C_{50S} - K_{f2}\Big(14C_{202S} + C_{606S}\Big)$$
$$- K_{b2}\Big(2C_{404S} + 15C_{505S}\Big) - K_{f3}\Big(0.25C_{04S} + C_{03S}\Big)$$
$$D_3 = \frac{7}{4}K_{f1} - K_{b1}\big(2C_{40S} + C_{50S}\big) + \frac{14}{16}K_{f2} - K_{b2}\Big(2C_{404S} + 15C_{505S}\Big) - 0.25K_{f3}$$
$$D_4 = -K_{b1} - \frac{30}{16}K_{b2}.$$

4.3 Analytical solution of the calcite rate law

The acid treatment model (calcite dissolution model) has an analytical solution which will be derived in this section for validation purposes.

Firstly, by substituting data (29) into Equation (8), we obtain mass balance expressions for the species in Equation (23) as follows:

$$[CaCO_3] = [CaCO_3]_0 - \chi. \tag{46}$$
$$[H^+] = [H^+]_0 - \chi. \tag{47}$$
$$[Ca^{2+}] = [Ca^{2+}]_0 + \chi. \tag{48}$$
$$[HCO_3^-] = [HCO_3^-]_0 + \chi. \tag{49}$$

Substituting expressions (46) – (49) into Equation (30) and manipulating the results, one obtains:

$$\frac{d\chi}{dt} = \mu_1 + \mu_2\chi - K_b\chi^2 \tag{50}$$

where

$$\mu_1 = K_f[H^+]_0 - K_b[Ca^{2+}]_0[HCO_3^-]_0, \quad \mu_2 = -(K_f + K_b[Ca^{2+}]_0 + K_b[HCO_3^-]_0)$$

are constants.

Equation (50) can be solved analytically (see, [37] for more details) to obtain:

$$\chi = \frac{\Theta_1\Theta_2\Big(1 - \exp^{-K_b(\Theta_1 - \Theta_2)t}\Big)}{\Theta_2 - \Theta_1\exp^{-K_b(\Theta_1 - \Theta_2)t}}. \tag{51}$$

where

$$\Theta_1 = \frac{-\mu_2 - \sqrt{\mu_2^2 + 4K_b\mu_1}}{-2K_b}, \quad \Theta_2 = \frac{-\mu_2 + \sqrt{\mu_2^2 + 4K_b\mu_1}}{-2K_b}.$$

Therefore, using (51) in (46) –(49) yields the following species concentration profiles:

$$[CaCO_3] = [CaCO_3]_0 - \frac{\Theta_1\Theta_2\left(1 - \exp^{-K_b(\Theta_1-\Theta_2)t}\right)}{\Theta_2 - \Theta_1 \exp^{-K_b(\Theta_1-\Theta_2)t}}, \tag{52}$$

$$[H^+] = [H^+]_0 - \frac{\Theta_1\Theta_2\left(1 - \exp^{-K_b(\Theta_1-\Theta_2)t}\right)}{\Theta_2 - \Theta_1 \exp^{-K_b(\Theta_1-\Theta_2)t}}, \tag{53}$$

$$[Ca^{2+}] = [Ca^{2+}]_0 + \frac{\Theta_1\Theta_2\left(1 - \exp^{-K_b(\Theta_1-\Theta_2)t}\right)}{\Theta_2 - \Theta_1 \exp^{-K_b(\Theta_1-\Theta_2)t}}, \tag{54}$$

$$[HCO_3^-] = [HCO_3^-]_0 + \frac{\Theta_1\Theta_2\left(1 - \exp^{-K_b(\Theta_1-\Theta_2)t}\right)}{\Theta_2 - \Theta_1 \exp^{-K_b(\Theta_1-\Theta_2)t}}. \tag{55}$$

Concentration and rate profiles for the species are given by Figure 1. Data from [31] was applied.

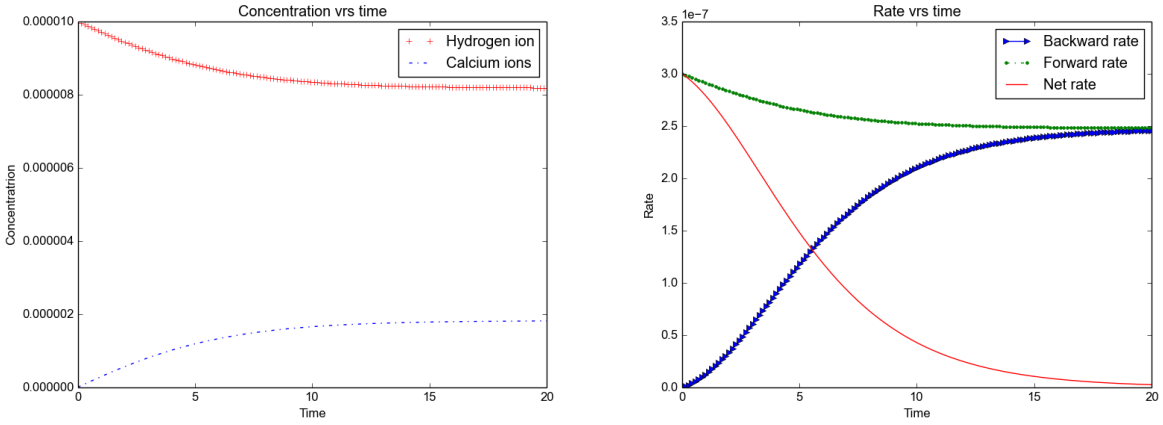

(a) Concentration profiles of species

(b) Rate of reaction profiles

Figure 1: Species concentration and rate profiles for Reaction (23).

Figure (1a) shows the changes in species concentration with time. The data used for generating the profiles contain a high concentration of hydrogen ions. It can be observed that while the concentration of H^+ (a reactant) decreases with time, the concentration of Ca^{2+} increases with time until equilibrium is reached.

Figure (1b) presents the evolution of the forward, backward and net rate profiles of calcite versus time. It can be observed that the expected profiles are reproduced: while the rate of dissolution is highest at the beginning of the reaction, the rate of precipitation is lowest at the beginning of the reaction. It can also be observed that while the rate of forward reaction decreases until equilibrium is achieved the rate of backward reaction increases with time until equilibrium is achieved. One more observation is that the net

rate of reaction is highest at the beginning but decreases to zero when equilibrium is reached. These observations conform with Le Chatelier's principle, and therefore, confirm the consistency of our analytical solution with the chemistry of the problem.

To test the accuracy of the stoichiometric decoupling method at the ordinary differential equation (ODE) level, we calculated the transient concentrations of the species H^+, Ca^{2+} and HCO_3^-, and with these values, we plotted rate against time, to obtain the rate profiles for both the single-variable ODEs and the original ODE.

In Figure 2c, we compare the transformed one-variable rate functions given by Equations (35), (36) and (37) to the original three variable ODE given by Equation (27).

From Figure 2c, it can be observed that the single-variable (stoichiometrically decoupled) ODEs given by Equations (35), (36) and (37) are the same as the original coupled ODE (27). We would like to point out that, each one of the modified ODEs (35), (36) and (37) depends on one variable only, thus we have a set of independent equations that represent the rate at which each species progresses in the calcite kinetics.

4.4 Other approximations for calcite kinetics

According to [33], the rate of calcite precipitation (backward reaction rate) can be approximated as follows:

$$K_b[Ca^{2+}][HCO_3^-] \approx 2K_b\big([Ca^{2+}]\big)^2, \tag{56}$$

or

$$K_b[Ca^{2+}][HCO_3^-] \approx 2K_b\big([HCO_3^-]\big)^2. \tag{57}$$

The approximations (56) and (57) have been verified in experiments involving pure water and calcite. By substituting Equation (56) into Equation (27), the calcite dissolution rate law becomes:

$$R_{CaCO_3} = K_f[H^+] - 2K_b\big([Ca^{2+}]\big)^2. \tag{58}$$

Similarly, substituting Equation (57) into Equation (27), the calcite dissolution rate law becomes:

$$R_{CaCO_3} = K_f[H^+] - 2K_b\big([HCO_3^-]\big)^2. \tag{59}$$

It is important to note here that, in the case of pure water-calcite kinetics, the rate law (27) with a three-variable rate function can be approximated by rate law (58) or (59) with two-variable rate functions. To investigate the accuracy of approximations (58) and (59), we compared their profiles with the original rate law (27) in Figure 2a.

From Figure 2a, one can observe that the approximations are reasonably accurate. However, further investigations revealed that the error depends on the ratio of input data (see Figure 2d or Table 2). We introduced a scalar ratio α_{sca}, such that:

$$[HCO_3^-]_0 + [Ca^{2+}]_0 = \alpha_{\text{sca}}[H^+]_0. \tag{60}$$

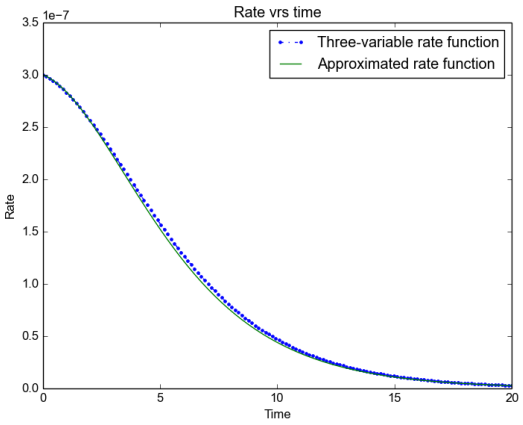

(a) Two-variable rate function

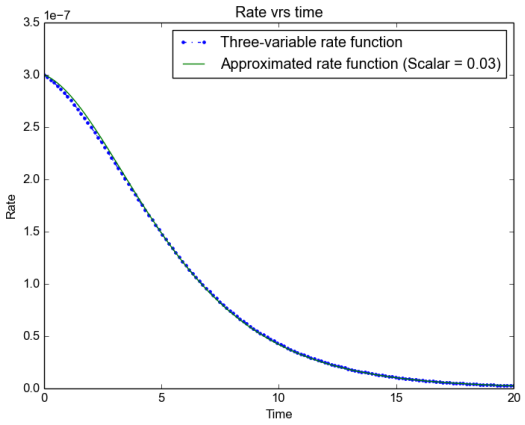

(b) Improved two-variable rate function

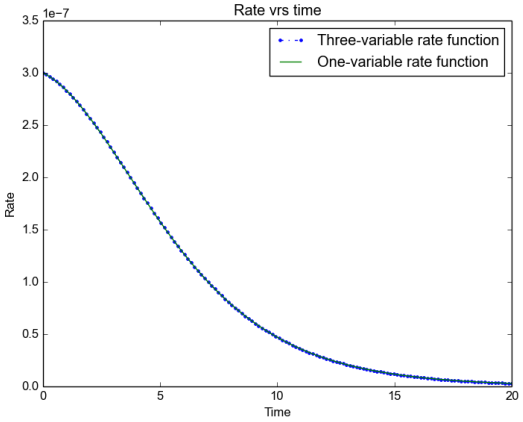

(c) One-variable rate function

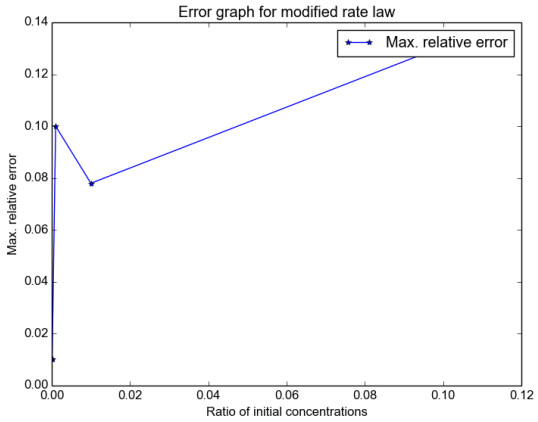

(d) Error profile for two-variable rate function

Figure 2: Profiles for the two-variable rate function (58) or (59), improved two-variable rate function (58) or (59), one-variable rate function (35) or (36) or (37) and errors of the two-variable rate functions, all profiles compared with the three-variable rate function (27).

Table 2: Error values for varying values of products and reactants input data.

Ratio of input data (α_{sca})	Maximum relative error
0.10000	0.1308
0.01000	0.0780
0.00100	0.1000
0.00010	0.1019
0.00001	0.01021

The ratio α_{sca} and maximum relative error was calculated from different input data values of $[HCO_3^-]_0$, $[H^+]_0$, and $[Ca^{2+}]_0$. Table 2, contains the calculated values for α_{sca} and the maximum relative error measured. In Figure 2b where $\alpha_{\text{sca}} = 0.03$, one can observe more accuracy than in Figure 2a where $\alpha_{\text{sca}} = 0.1$.

However, calcite dissolution and precipitation occurs naturally and one can not control the input data or ensure that reaction occurs in pure water. Besides, the approximations are two-variable functions, which lead to coupling. Thus the models given by rate laws (58) and (59), will not always be useful as compared with the stoichiometrically decoupled model given by rate function (35) especially in modelling studies.

5 Numerical schemes

Notable challenges with stoichiometrically decoupled models is non-linearity that makes exact solutions infeasible. In this Section, we discuss some numerical schemes that will be used to analyse the stoichiometrically decoupled models. We present low and high order implicit one-step (Runge-Kutta and Rosenbrock) schemes that are suitable for stiff problems. We also present positivity-preserving schemes that are conservative and suitable for chemical kinetic problems.

After applying the model reduction methods discussed in Section 3, the resulting models satisfy the general form:

$$\frac{dU_k}{dt} = F_k(t, U_k), \qquad t \in [0, T), \qquad \mathbf{U}(0) = \mathbf{U}_0, \quad k = 1, 2, \ldots, N. \tag{61}$$

where U_k is current concentration of species k, $F_k(t, U_k)$ is the rate function of species k, and $\mathbf{U}_0$ is initial data of all the species. In Equation (61) we made F_k a function of time, for the sake of completeness in our presentation of Runge-Kutta schemes.

5.1 Runge-Kutta schemes

A generalized Runge-Kutta scheme for the initial-value problem (61), states that [26]:

$$U_k^{n+1} = U_k^n + \Delta t \sum_{i=1}^{m} q_i F_k(t_n + r_i \Delta t, U_{ni}), \tag{62}$$

$$U_{ni} = U_k^n + \Delta t \sum_{j=1}^{m} \alpha_{ij} F_k(t_n + r_i \Delta t, U_{ni}), \quad i = 1, 2, \ldots, m, \tag{63}$$

where m is the number of stages, $\Delta t = \frac{T}{N_t}$ is the time step size, N_t is total number of time steps and $t_n = n\Delta t$ is the n^{th} time point in the discrete time interval, $U_k^n = U_k(t_n)$ and $U_k^{n+1} = U_k(t_{n+1})$. Specifying the coefficients α_{ij}, q_i will define a particular method. The coefficients $r_i = \sum_{j=1}^{m} \alpha_{ij}$, for $i = 1, 2, \ldots, m$. It is convenient to represent a particular Runge-Kutta method in a compact/tabular form, called Butcher's array (see Table 3a for the tabular form of general Runge-Kutta method).

We will now apply three implicit Runge-Kutta schemes to solve ODE (35) where $U_k = [H^+]$ and $F_k(t, U_k) = -K_b U_k^2 + \lambda_3 U_k - \lambda_4$. The first particular scheme that will be applied is called Backward Euler or implicit Euler. It is one-stage ($m = 1$), unconditionally stable, first-order consistent and has the following Butcher's array [26] given by Table 3b.

Table 3: Butcher arrays for Runge-Kutta methods

r_1	α_{11}	$\cdots$	α_{im}
$\vdots$	$\vdots$	$\vdots$	$\vdots$
r_m	α_{m1}	$\cdots$	α_{mm}
	q_1	$\cdots$	q_m

(a) Butcher array

1	1
	1

(b) Euler

$\frac{1}{3}$	$\frac{5}{12}$	$-\frac{1}{12}$
1	$\frac{3}{4}$	$\frac{1}{4}$
	$\frac{3}{4}$	$\frac{1}{4}$

(c) Radau

$\frac{1}{2}-\frac{1}{6}\sqrt{3}$	$\frac{1}{4}$
$\frac{1}{2}+\frac{1}{6}\sqrt{3}$	$\frac{1}{4}+\frac{1}{6}\sqrt{3}$
	$\frac{1}{2}$

(d) Gauss

The second scheme that will be applied is the two-stage Gauss quadrature scheme. It is unconditionally stable, fourth-order consistent and has the following Butcher's array [26] given by Table 3d:

The third implicit Runge-Kutta scheme applied is the two-stage Radau quadrature scheme. It is unconditionally stable, third-order consistent and has the following Butcher's array [26] given by Table 3c:

5.2 Rosenbrock schemes

A generalized Rosenbrock scheme of any order, for the autonomous case of the initial-value problem (61) states that [26]:

$$U_k^{n+1} = U_k^n + \sum_{i=1}^{m} q_i U_{ni}, \tag{64}$$

$$U_{ni} = \Delta t\ F_k(U_k^n + \sum_{j=1}^{i-1} \alpha_{ij} U_{nj}) + \Delta t\ F_k'(U_k^n) \sum_{j=1}^{i} \gamma_{ij} U_{nj}, \quad i = 1, 2, \ldots, m, \tag{65}$$

where $F_k'(V^n)$ is the Jacobian of $F_k(U_k^n)$, and the coefficients $q_i, \alpha_{ij}, \gamma_{ij}$ determine the order of consistency and stability of a particular Rosenbrock method.

In this discussion, we only consider three particular Rosenbrock schemes. The first scheme (code named *Rose1*) is one stage, first order consistent (with $\gamma_{11} = 1$) and $L-$stable given by [26]:

$$U_k^{n+1} = U_k^n + U_{n1}, \tag{66}$$

$$U_{n1} = \Delta t\ F_k(U_k^n) + \Delta t\ F_k'(U_k^n)\gamma_{11} U_{n1}. \tag{67}$$

The second scheme (code named *Rose2*) has two stages, is second order consistent and $L-$stable (with $\gamma_{11} = \gamma_{22} = 1 + 0.5\sqrt{2}$) given by [26]:

$$U_k^{n+1} = U_k^n + 0.5U_{n1} + 0.5U_{n2}, \tag{68}$$

$$U_{n1} = \Delta t\ F_k(U_k^n) + \Delta t\ F_k'(U_k^n)\gamma_{11} U_{n1}, \tag{69}$$

$$U_{n2} = \Delta t\ F_k(U_k^n + U_{n1}) - 2\Delta t\ F_k'(U_k^n)\gamma_{11} U_{n1} + \Delta t\ F_k'(U_k^n)\gamma_{22} U_{n2}. \tag{70}$$

The third scheme (code named *Rose3*) has two stages, is third order consistent and strongly $A-$stable (with $\gamma_{11} = \gamma_{22} = 0.5 + \frac{1}{6}\sqrt{3}$) given by [26]:

$$U_k^{n+1} = U_k^n + 0.25U_{n1} + 0.75U_{n2}, \tag{71}$$

$$U_{n1} = \Delta t\ F_k(U_k^n) + \Delta t\ F_k'(U_k^n)\gamma_{11}U_{n1}, \tag{72}$$

$$U_{n2} = \Delta t\ F_k(U_k^n + \frac{2}{3}U_{n1}) - \frac{4}{3}\Delta t\ F_k'(U_k^n)\gamma_{11}U_{n1} + \Delta t\ F_k'(U_k^n)\gamma_{22}U_{n2}. \tag{73}$$

5.3 Positivity-preserving schemes

The positivity-preserving class of schemes we will consider for the autonomous case of Equation (61) is the Theta class which states that [24]:

$$U_k^{n+1} - \theta\Delta t\ F_k(U_k^{n+1}) = U_k^n + (1-\theta)F_k(U_k^n), \tag{74}$$

where θ is the parameter that determines specific schemes.

The first scheme in this class that will be considered in the discussion is $\theta = 0$, called the explicit Euler scheme. This scheme is conditionally stable, first-order consistent, conservative and positivity-preserving.

The second scheme that we consider is $\theta = 1$ called the implicit Euler schemes. This scheme is unconditionally stable, first-order consistent, conservative and positivity-preserving.

The third positivity-preserving scheme is $\theta = \frac{1}{2}$ called the Crank-Nicholson (also referred to as *Nicholson* below) scheme. This scheme is unconditionally stable, second order consistent, conservative and positivity-preserving.

For a detailed discussion on convergence, positivity, conservation and absolute stability refer to [24, 26, 34].

6 Numerical experiments

In this Section, we present results from numerical experiments, obtained by applying the numerical schemes (presented in Section 5) to the stoichiometrically decoupled calcite model presented in Section 3. The goal is to quantify numerical errors in the reduced model (which implicitly contain the stoichiometric reduction error) at the species profile level, in order to validate and establish the suitability of the numerical schemes and the compatibility of the stoichiometric decoupling/reduction method. Section 6.1 contains discussion on convergence of the numerical schemes. Section 6.2 contains discussion on accuracy of the decoupling methods and Section 6.3 contains discussion on cost of simulation.

6.1 Convergence test for numerical schemes

The numerical solutions obtained by applying the Runge-Kutta, Rosenbrock and Theta classes of schemes to ODE (35), have been compared with the exact solution in Figure 3. Table 4 contains error values for all the classes, these were measured across time steps and norms. The error values are 10^{-7} orders of magnitude, thus are very small. From

Figure 3 and Table 4, one can observe that errors are decreasing monotonically for all the numerical schemes.

In summary, the errors of all the numerical schemes (Runge-Kutta, Rosenbrock and Theta schemes) decrease monotonically across time steps, which implies that the schemes are accurate and convergent. This further implies that the stoichiometric reduction method does not negatively affect the performance of the numerical schemes. The results also show that the high-order schemes (Radau, *Rose3* and Crank-Nicholson) performed better.

Table 4: Errors of the numerical schemes measured across norms and time steps. The numerical values in this table are of order 10^{-7}.

Runge-Kutta schemes					
Error norms	Numerical schemes	Time steps			
		$N_t = 5$	$N_t = 10$	$N_t = 15$	$N_t = 20$
$\|\cdot\|_\infty$	Backward Euler	1.7600	0.9910	0.6841	0.5208
	2-stage Gauss	0.0671	0.0223	0.0107	0.0063
	2-stage Radau	0.0662	0.0137	0.0056	0.0031
$\|\cdot\|_2$	Backward Euler	2.7503	2.0436	1.6992	1.4856
	2-stage Gauss	0.0930	0.0421	0.0246	0.0165
	2-stage Radau	0.0923	0.0271	0.0137	0.0086
Rosenbrock schemes					
Error norms	Numerical schemes	Time steps			
		$N_t = 5$	$N_t = 10$	$N_t = 15$	$N_t = 20$
$\|\cdot\|_\infty$	*Rose1*	0.6962	0.6747	0.5310	0.4338
	Rose2	0.5713	0.3515	0.2192	0.1485
	Rose3	0.2267	0.0459	0.0161	0.0074
$\|\cdot\|_2$	*Rose1*	1.0864	1.3846	1.3242	1.2356
	Rose2	0.8530	0.7160	0.5438	0.4245
	Rose3	0.3011	0.0884	0.0315	0.0203
Theta schemes					
Error norms	Numerical schemes	Time steps			
		$N_t = 5$	$N_t = 10$	$N_t = 15$	$N_t = 20$
$\|\cdot\|_\infty$	Implicit Euler	1.7600	0.9910	0.6841	0.5208
	Explicit Euler	2.7794	1.2604	0.7965	0.5857
	Crank-Nicholson	0.1823	0.0502	0.0235	0.0129
$\|\cdot\|_2$	Implicit Euler	2.7503	2.0436	1.6993	1.4856
	Explicit Euler	3.6038	2.3211	1.8487	1.5824
	Crank-Nicholson	0.2427	0.0863	0.0467	0.0303

6.2 Accuracy test on the decoupling methods

In this Section, we present convergence results for the stoichiometric decoupling, Gauss-Seidel (also referred to as G. Seidel below), Gauss-Jacobi (also referred to as G. Jacobi below) and Successive-Over-Relaxation (SOR) decoupling methods discussed earlier in

Section 3. The goal is to compare the performance of the stoichiometric method with the other methods.

When $\omega = 0$, the Successive-Over-Relaxation (SOR) reduces to Gauss-Seidel. Results from our experiments (see Table 5) show that when $\omega = 0.1$ the SOR approach performs well.

All the numerical schemes (Runge-Kutta, Rosenbrock and Theta schemes) discussed in Section 6 were applied to all the models resulting from all the decoupling methods (discussed in Section 3) to obtain corresponding discrete versions. However, we only present results for Radau, *Rose3* and Crank-Nicholson schemes, since they performed better than the other schemes.

The errors of the numerical schemes (applied on the stoichiometrically decoupled model (35) and the Gauss-Seidel, Gauss-Jacobi and Successive-Over-Relaxation (SOR) decoupling of (31)-(33)) were measured relative to the analytical solution in Equation (53). Table 6 contains errors of the numerical schemes (Radau, *Rose3* and Crank-Nicholson schemes) measured across increasing time steps. Figure 4 shows the error profiles of the Radau, *Rose3* and Crank-Nicholson schemes applied on all the decoupled models. It can be observed in Figure 4 and Table 6, that all the numerical schemes had minimal errors when applied to the stoichiometrically decoupled model. Relative to Gauss-Seidel and SOR decoupling, the Gauss-Jacobi decoupling method performed better.

Table 5: Errors ($\|\cdot\|_\infty$) of the Radau, *Rose3*, and Crank-Nicholson schemes, applied to the SOR decoupling of the large model (31)-(33), using different values of the parameter ω, $N_t = 15$ and all other model parameters held constant.

ω	0.9	0.5	0.2	0.1	0.01	0.001	0.0001
Radau	13.1470	5.3289	2.3859	2.0054	2.2302	2.2545	2.2570
Rose3	13.1387	5.3035	2.3397	1.7912	1.8433	1.8674	1.8698
Crank-Nicholson	13.1384	5.3056	2.3463	1.8111	1.8619	1.8803	1.8821

6.3 Experiments on cost of simulation

In the Section, we present and discuss results on cost of simulation, using two chemical kinetic models. The first model is the calcite (acid neutralization) model presented in Section 4.1, and the second model is pyrite oxidation (acid generation) model presented in Section 4.2. The experiments were performed using *Radau,* Rose3 *and Crank-Nicholson* discretizations for the two models. CPU time, CPU time differences and relative CPU time were obtained for all the decoupling methods, using grid refinement tests. Throughout this Section, we define CPU time differences and relative CPU time as follows:

$$\text{CPU time difference} = \text{CPU}_C - \text{CPU}_S \tag{75}$$

and

$$\text{Relative CPU time} = \frac{\text{CPU}_C - \text{CPU}_S}{\text{CPU}_C} \tag{76}$$

Table 6: Errors of the large linear model (30)-(33) and reduced non-linear model (35), computed across numerical schemes, norms and time steps. The numerical values in this table are of order 10^{-7}.

Scheme	Norms	Method	Time steps			
			$N_t = 15$	$N_t = 20$	$N_t = 30$	$N_t = 50$
2-stage Radau	$\|\cdot\|_\infty$	Gauss-Jacobi	0.6317	0.4761	0.3181	0.1910
		Gauss-Seidel	2.2572	1.6771	1.1078	0.6599
		SOR ($\omega = 0.1$)	2.0054	1.5405	1.2316	1.0266
		Stoichiometric	0.0056	0.0031	0.0013	0.0005
	$\|\cdot\|_2$	Gauss-Jacobi	1.5754	1.3861	1.1499	0.9020
		Gauss-Seidel	6.4410	5.4760	4.3879	3.3509
		SOR ($\omega = 0.1$)	6.7605	6.2086	5.7473	5.6304
		Stoichiometric	0.0137	0.0086	0.0045	0.0020
Rose3	$\|\cdot\|_\infty$	Gauss-Jacobi	0.6878	0.5187	0.3478	0.2097
		Gauss-Seidel	1.8701	1.3936	0.9233	0.5513
		SOR ($\omega = 0.1$)	1.7912	1.4859	1.2055	1.0128
		Stoichiometric	0.0161	0.0074	0.0024	0.0006
	$\|\cdot\|_2$	Gauss-Jacobi	1.9798	1.7500	1.4567	1.1449
		Gauss-Seidel	5.7238	4.8814	3.9252	3.0037
		SOR ($\omega = 0.1$)	6.1228	5.7060	5.3798	5.3854
		Stoichiometric	0.0382	0.0203	0.0081	0.0024
Crank-Nicholson	$\|\cdot\|_\infty$	Gauss-Jacobi	0.6867	0.5179	0.3474	0.2095
		Gauss-Seidel	1.8823	1.4004	0.9263	0.5524
		SOR ($\omega = 0.1$)	1.8111	1.4859	1.2055	1.0392
		Stoichiometric	0.0235	0.0129	0.0059	0.0021
	$\|\cdot\|_2$	Gauss-Jacobi	1.9669	1.7405	1.4508	1.1419
		Gauss-Seidel	5.7530	4.8997	3.9348	3.0080
		SOR ($\omega = 0.1$)	6.2414	5.7855	5.4312	5.4137
		Stoichiometric	0.0467	0.0303	0.01643	0.0076

where CPU_S is the CPU time for the stoichiometric method and CPU_C is the CPU time for any of the other methods. In the experiments, we fixed the final time at $T = 20$ and use a very fine grid (8000 time steps) to ensure that results are not affected much by numerical discretization errors.

6.3.1 Acid neutralization (calcite) model

The final time was set at $T = 20$, *Radau,* Rose3 *and Crank-Nicholson* discretization schemes were applied to the calcite model, CPU time for all the decoupling techniques were obtained by varying the grid resolution. Figures 5a, 5c and 5e show plots of CPU time against time steps, obtained in the *Radau,* Rose3 *and Crank-Nicholson* discretizations, for all the decoupling techniques. In all the discretizations, the CPU time for all the decoupling techniques generally increased with increasing time steps, however, the CPU time for the stoichiometric technique recorded the least CPU time. Another observation is

that, the CPU time difference between the stoichiometric method and the other methods increased with increasing time steps, in all the discretization schemes. This observation can be seen clearly in Figures 5b, 5d and 5f. One other observation is that, the CPU time and differences vary across the numerical discretizations, this is because the *number of terms to evaluate* and the *number of iterations to converge* vary across discretizations, but greatly influence simulation time.

6.3.2 Pyrite oxidation model

It is not trivial to obtain an analytical solution of this system (presented in Section 4.2) and solving it numerically without applying model reduction methods would be impractical. Thus *Gauss-Seidel, Gauss-Jacobi and SOR methods* are applied to decouple Equation (44) before solving numerically. We compare results for the stoichiometric method with the results of *Gauss-Seidel, Gauss-Jacobi and SOR methods*. The following input data was used in simulating the pyrite model:

$$\begin{aligned} &K_{f1} = 0.7, \quad K_{b1} = 0.007, \quad K_{f2} = 0.03, \quad K_{b2} = 0.007, \quad K_{f3} = 0.02 \\ &\mathbf{U}_0 = (0.000001, 1, 0.02, 0.002, 0.00001, 0.003)^{\mathrm{Tr}} \quad \text{and} \\ &\mathbf{U}_S = (0., 0., 0., 0., 0., 0.)^{Tr}. \end{aligned} \tag{77}$$

During oxidation, the concentration of the hydrogen ion is expected to rise until equilibrium, where the concentration profile becomes independent of time and time-grid resolutions. Figures 6a and 6b show expected transient and equilibrium concentration profiles in the Crank-Nicholson and *Rose3* discretizations, for all the decoupling methods. However, the equilibrium concentration predicted by the stoichiometric method remained constant with grid-refinement, while the equilibrium concentration predicted by the other decoupling methods varied with grid resolution, see Figure 6. Moreover, the equilibrium values predicted by the other methods eventually converge (using 8000 time steps and above) to the value predicted by the stoichiometric method (see Figures 6e and 6f). This observation supports our earlier results that the stoichiometric method is more accurate, accelerates convergence and is compatible with numerical schemes.

Next, *Radau,* Rose3 *and Crank-Nicholson* discretization schemes were applied to the pyrite model. The CPU time for all the decoupling methods was measured for different time-grid resolutions. Figure 7 shows the results of the experiments. The observations are not very different from those in the calcite model. In all the discretizations, the CPU time (see Figures 7a, 7c and 7e) and CPU time differences (see Figures 7b, 7d and 7f) for all the decoupling methods generally increased with increasing time steps, however, the CPU time for the stoichiometric method recorded the least values.

6.3.3 Relative cost of simulation

In order to determine the CPU time saved by using stoichiometric decoupling instead of the other methods, the CPU time differences for the *Gauss-Jacobi, Gauss-Seidel and SOR* decoupling methods (measured across the *Radau,* Rose3 *and Crank-Nicholson* discretizations of both calcite and pyrite models) were divided by the CPU time for *Gauss-Jacobi, Gauss-Seidel and SOR* (i.e., using Equation (76)). Figure 8 shows the results of the investigation.

In the calcite model, when stoichiometric decoupling is applied with *Radau* discretization, *82 percent* of the CPU time of the other decoupling methods will be saved, *84 percent* if *Rose3* discretization is used, and *96 percent* if *Crank-Nicholson* is used (see Figures 8a, 8c and 8e).

In the pyrite model, applying stoichiometric decoupling with *Radau* discretization will save up to *82 percent* of the CPU time for the other decoupling methods, save *88 percent* if *Rose3* discretization is used, and *97 percent* if *Crank-Nicholson* is used (see Figures 8b, 8d and 8f). The pyrite system in Equation (44) has more terms to evaluate than the stoichiometric case in Equation (45) especially when a fine grid is used.

Another observation is that, in both calcite and pyrite models, the CPU time saved by using *Radau* and *Rose3* discretizations are lower compared to *Crank-Nicholson* discretizations. This is because the *Radau* and *Rose3* discretizations have two stages of evaluations that introduce extra terms into the computation (unlike *Crank-Nicholson* that has one stage). Thus, applying *Crank-Nicholson* on the stoichiometric models result in faster computations than the *Radau* and *Rose3* schemes. The faster computations result in less CPU time, larger CPU time differences (see Figures 5 and 6) and higher relative CPU time. This explains why the CPU time saved (relative CPU time) in the *Crank-Nicholson* discretization is higher in both models (see Figure 8).

7 Conclusion

Most chemical processes are complicated, difficult to model and expensive to simulate. Such complications result from large numbers of species involved in many reactions at varying time-scales. Efficient model reduction methods are required to reduce computational cost and still maintain high accuracy. Many researchers have developed various reduction strategies that are based on decoupling species or reactions, but not much has been done to address the case where the rate profiles of some of the many species are of interest.

In this discussion, we first presented a decoupling method (see Section 3) that is based on stoichiometry and mass balances. The method can be applied to any stoichiometric system (where the profiles of some of the many species are of interest) to significantly reduce computational cost and maintain high accuracy.

Secondly, we applied the method to calcite dissolution and pyrite oxidation kinetics to reduce their degrees of freedom from four to one and six to one, respectively. The evidence provided by the calcite model at the ODE level (see Section 4), shows that the stoichiometric method maintains the physical and chemical essential features of the original system. The results also show a remarkable accuracy of the method (at the ODE level) as compared with other reduction methods.

Thirdly, we numerically simulated (at the species-concentration level) the stoichiometrically decoupled models for the acidic effluent generation/treatment, in order to establish compatibility with numerical schemes. The sum of all errors (including rounding, truncation and model reduction errors) is 10^{-7} orders of magnitude, and generally decreases monotonically with increasing time steps. This evidence provided in Sections 6.1 shows that, the model reduction error does not significantly affect the overall error, which implies that the method is compatible with the numerical schemes. This observation also implies

that the stoichiometric decoupling method is accurate at the species-concentration level.

Fourthly, we compared the performance of the stoichiometric decoupling method with three other methods (namely Gauss-Seidel, Gauss-Jacobi and Successive-Over-Relaxation (SOR)), by checking the rate at which numerical schemes converged to the analytical solution in all the decoupled models (see Section 6.2). The numerical errors in the stoichiometrically decoupled model are orders of magnitude smaller than those of the other models. The results further show that the numerical solutions of the stoichiometrically decoupled model converges faster than the numerical solutions of the other decoupled models. Thus stoichiometric decoupling is compatible with numerical schemes and can accelerate convergence of the numerical scheme.

Fifthly, we presented and discussed results on cost of simulation, using two chemical kinetic models (see Section 6.3). CPU time, CPU time differences and relative CPU time were measured and compared for all the decoupling methods and numerical schemes. The results showed that stoichiometric decoupling can significantly reduce cost of simulation.

Therefore, with the evidence provided above, we conclude that the stoichiometric decoupling method is an efficient method for reducing the computational cost of chemical kinetic models, especially when some of the many species are of interest.

Acknowledgement

EAA acknowledges support from the Pilot Bursary of the University of Pretoria, the African Institute of Mathematical Sciences and University of Stellenbosch. MKB is grateful to the African Institute for Mathematical Sciences (AIMS) for hosting him while finalising this work. This work is also supported in part by the National Research Foundation of South Africa (Grant number: 93099 and 93476).

References

[1] D. Kirk Nordstrom, "Hydrogeochemical processes governing the origin, transport and fate of major and trace elements from mine wastes and mineralized rock to surface waters", Applied Geochemistry 26, 1777-1791 (2011).

[2] Chen Zhu, Fang Q. Hu, and David S. Burden,"Multi-component reactive transport modeling of natural attenuation of an acid groundwater plume at a uranium mill tailings site", Journal of Contaminant Hydrology 52, 85-108 (2001).

[3] D. Kirk Nordstrom, David W. Blowes, and Carol J. Ptacek,"Hydrogeochemistry and microbiology of mine drainage: An update", Applied Geochemistry 57, 3-16 (2015).

[4] K. S. Shabani, F. D. Aredejani, R.N. Singh, and R. Marandi, H. Soleimanyfar, "Numerical Modeling of Cu^{2+} and Mn^{2+} ions biosorption by Aspergillus niger fungal biomass in a continuous reactor", Arch. Min. Sci. 56, 461-476 (2011).

[5] Petzold, L. and Zhu, W., "Model Reduction for Chemical Kinetics: An Optimization Approach", AIChE Journal 45(4) (1999) pp. 869 – 886.

[6] Peters N., "Reduced Mechanisms In: Smooke, M.D. (Ed.), Reduced Kinetic Mechanisms and Asymptotic Approximations for Methane-Air Flames", Lecture Notes in Physics, Berlin-Heidelberg, Springer-Verlag 384 (1991), DOI: 10.1007/BFb0035362.

[7] Williams F. A., "Combustion Theory, The Fundamental Theory of Chemically Reacting Systems", 2nd ed., Menlo Park, CA, Benjamin Cummings Publishing Co. (1985).

[8] Peters N., "Numerical and Asymptotic Analysis of Systematically Reduced Reaction Schemes for Hydrocarbon Flames," In: Glowinski, L. and Temam, R. (Eds.), Numerical simulation of combustion phenomena, Lecture Notes in Physics, Springer Verlag Berlin 241 (1985) pp. 90 – 109.

[9] Carr Jr. R. W., Peterson D. G. and Smith F. K., "Flash Photolysis of 1,3-Dichlorotetrafluoroacetone in the Presence of Oxygen, Kinetics and Mechanism of the Oxidation of the Chlorodifluoromethyl Radicals", J. of Phys. Chem. 90 (1986) pp. 607 – 614.

[10] Seigneur C., Stephanopoulos G. and Carr Jr. R. W., "Dynamic Sensitivity Analysis of Chemical Reaction Systems: a variational method", Chem. Eng. Sci. 37(6) (1982) pp. 845 – 853.

[11] Gautier O., Carr Jr. R. W. and Seigneur C., "Variational Sensitivity Analysis of a Photochemical Smog Mechanism", Int. J. of Chemical Kinetics 17(12) (1985) pp. 1347 – 1364, DOI: 10.1002/kin.550171211.

[12] Allara D. L. and Edelson D., "A Computational Modeling Study of the Low-Temperature Pyrolysis of n-Alkanes; Mechanisms of Propane, n-Butane, and n-Pentane Pyrolyses," Int. J. Chem. Kinet. 7 (1975) pp. 479 –507.

[13] Brown N. J., Li G. and Koszykowski M. L., "Mechanism Reduction via Principal Component Analysis," Int. J. Chem. Kinet. 29(6) (1997) pp. 393 – 414.

[14] Edelson D., "Computer Simulation in Chemical Kinetics", Science 214 (1981) pp. 981 – 986.

[15] Lam S. H., "Using CSP to understand complex chemical kinetics," Combust. Sci. and Tech. 89 (1993) pp. 375 – 404.

[16] Lam S. H. and D. A. Goussis, "Conventional Asymptotics and Computational Singular Perturbation for Simplified Kinetics Modelling," In: Smooke, M.D. (Ed.), Reduced kinetic mechanisms and asymptotic approximations for Methane-Air flames, Springer Verlag, Berlin (1991).

[17] Maas U. and Pope S. B., "Simplifying Chemical Kinetics: Intrinsic Low-Dimensional Manifolds in Composition Space", Combustion and Flame 88 (1992) pp. 239 – 264.

[18] Vajda S., Valko P. and Turanyi T., "Principal Component Analysis of Kinetic Models," Int. J. of Chem. Kin. 17 (1) (1985) pp. 55 – 81, DOI: 10.1002/kin.550170107.

[19] Grimme E., "An Implicitly Restarted Lanczos Method for the Model Reduction of Stable Large-Scale Systems," MS Thesis, Univ. of Illinois at Urbana-Champaign, IL, (1993).

[20] Grimme E., Sorensen D. and Van Dooren P., "Stable Partial Realizations via an Implicitly Restarted Lanczos Method," Proc. Amer. Control Conf., Baltimore, MD, (1994).

[21] Arthur M. Lesk, Introduction to physical Chemistry, Prentice-Hall, Inc (982), ISBN 0-13-492710-9.

[22] Atkins P. W., Physical Chemistry, third edition, Oxford University Press (1987), ISBN 0-19-855196-7.

[23] Ira N. Levine, Physical Chemistry, third edition,McGraw-Hill, Inc (1978), ISBN 0-07-037474-0.

[24] Formaggia L. and Scotti A., Positivity and conservation properties of some integration schemes for mass action kinetics, SIAM J. NUMER. ANAL. Vol 49, No. 3, (2011), pp 1267-1288

[25] Walter J. Moore, Physical Chemistry, fifth edition, Prentice-Hall, Inc. (1972), ISBN 0-5824-44234-6

[26] Willem Hundsdorfer and Jan Verwer, "Numerical Solution of Time-Dependent Advection-Diffusion-Reaction Equations", Springer-Verlag Berlin Heidelberg, New York, (2003), ISBN 978-3-642-05707-6.

[27] Bellen A., Jackiewicz Z. and Zennaro M., Contractivity of waveform relaxation Runge-Kutta iterations and related limit methods for dissipative systems in the maximum norm, SIAM J. NUMER. ANAL. Vol. 31, No. 2, (1994) pp. 499-523

[28] Reddy M. M., Plummer L. N. and Busenberg E., "Crystal growth of calcite from calcium bicarbonate solution at constant P_{CO_2} and 25^oC : a test of calcite dissolution model", Geochimica et Cosmochimica Acta 45 (1981) pp. 1281–1289.

[29] Plummer L. N., Wigley T. M. L. and Parkhurst D. L., "The kinetics of calcite dissolution in CO_2- water systems at 5^oC to 60^oC and 0.0 to 1.0 atm CO_2", Am. J. Sci. 278 (1978) pp. 179–216, DOI:10.2475/ajs.278.2.179.

[30] Stumm W. and Morgan J. J., "Aquatic Chemistry: An introduction emphasizing chemical equilibria in natural waters", New York, NY: Wiley-Interscience (1970).

[31] Stumm, W., Lee, G. F., "Oxygenation of Ferrous Iron", Ind. Eng. Chem. (1961), 53(2), pp. 143–146, DOI: 10.1021/ie50614a038.

[32] Langmuir D., "Aqueous Environmental Geochemistry", New York, NY: Prentice-Hall, Inc. (1997).

[33] Appelo C. A. J. and Verweij, E., Schäfer, H., "A hydrogeochemical transport model for an oxidation experiment with pyrite/calcite/exchangers/organic matter containing sand", Appl. Geochemistry 13(2) (1998) pp. 257–268.

[34] Quarteroni A., Sacco R., and Saleri F., Numerical Mathematics, Springer-Verlag, Berlin, 2007.

[35] Garrels R. M. and Thompson M. E., Oxidation of pyrite by iron sulphate solution, American Journal of Science 258 (1960) pp. 57–67

[36] Singer P. C. and Stumm W., Acidic Mine Drainage, the rate determining step, Science 167 (1970) pp. 1121–1123.

[37] Boyce, W.E. and DiPrima R.C., Elementary differential equations and boundary value problems, Wiley, New York, 2012.

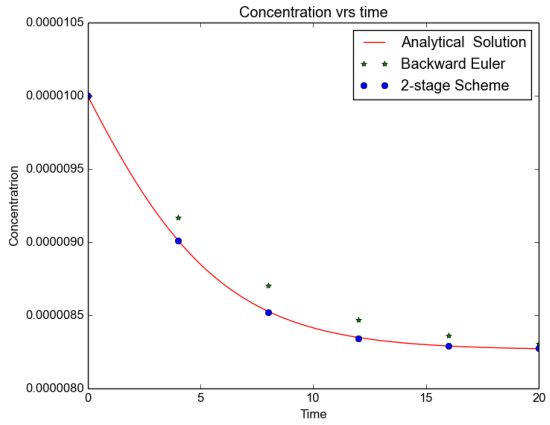

(a) Runge-Kutta/five time steps.

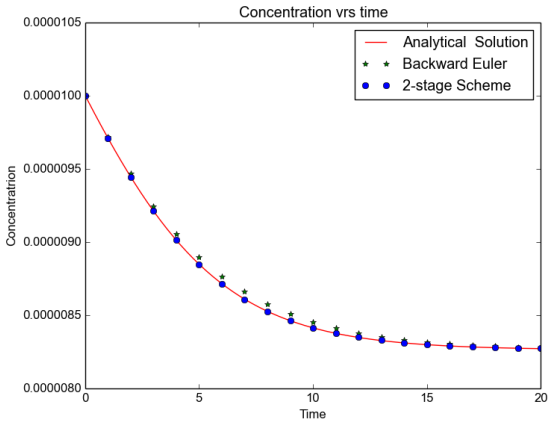

(b) Runge-Kutta/twenty time steps.

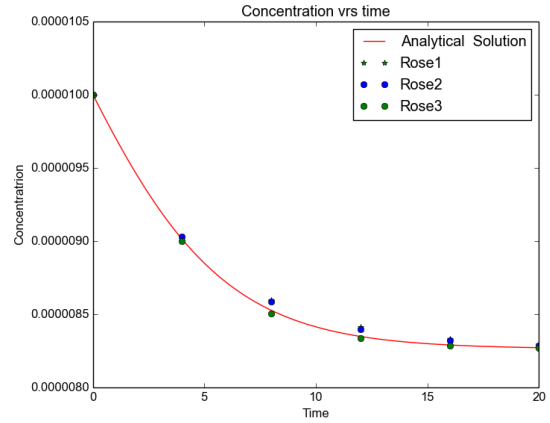

(c) Rosenbrock/five time steps.

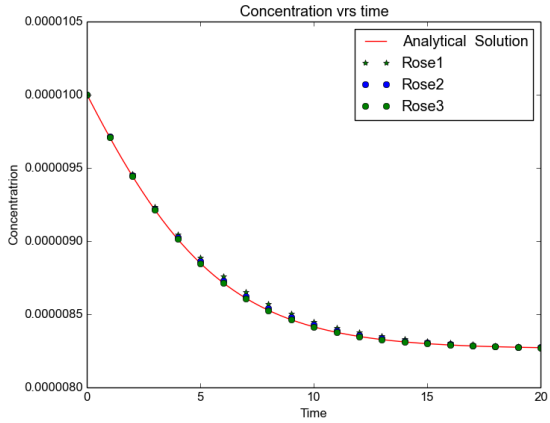

(d) Rosenbrock/twenty time steps.

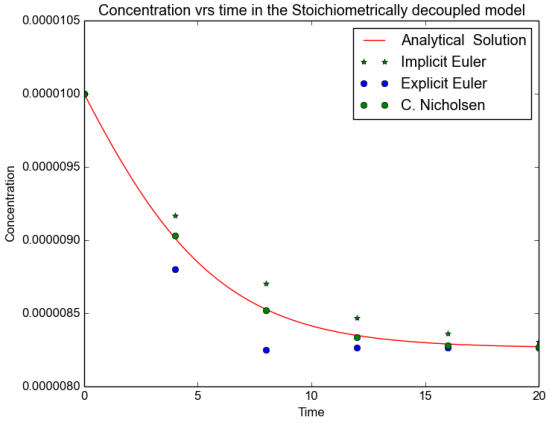

(e) Theta/five time steps.

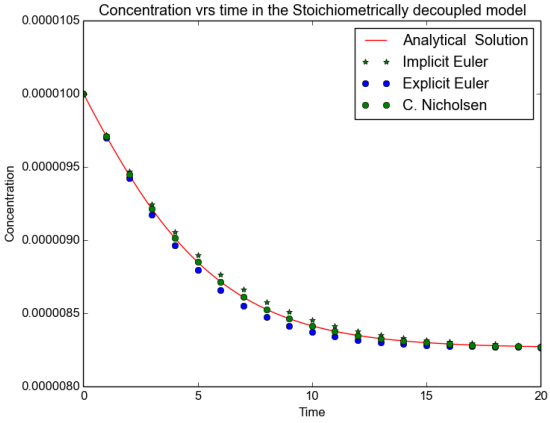

(f) Theta/twenty time steps.

Figure 3: Numerical and analytical solutions for ODE (62), where $U_k = [H^+], T = 20, [H^+]_0 = 10^{-5}$, and $F_k(t, [H^+]) = -K_b[H^+]^2 + \lambda_3[H^+] - \lambda_4$. The analytical solution is Equation (53).

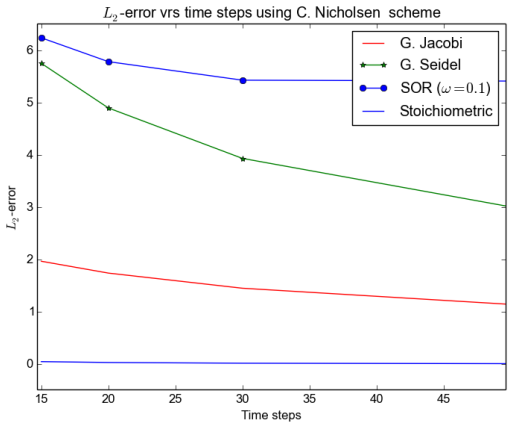

(a) L_2- errors, using Crank-Nicholson scheme.

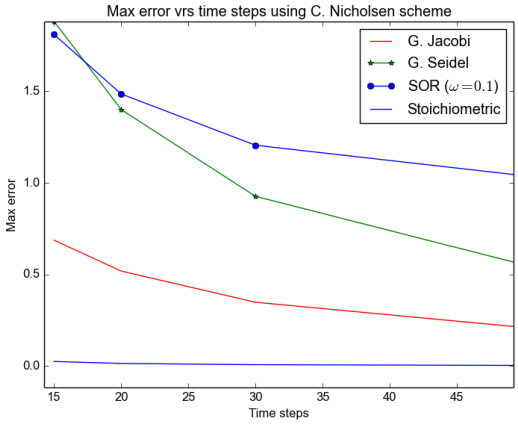

(b) Max. errors, using Crank-Nicholson scheme.

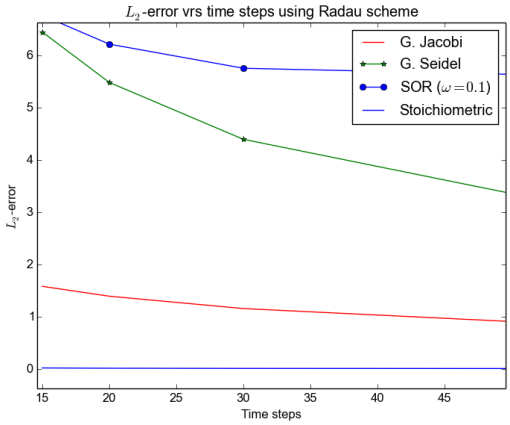

(c) L_2- errors, using Radau scheme.

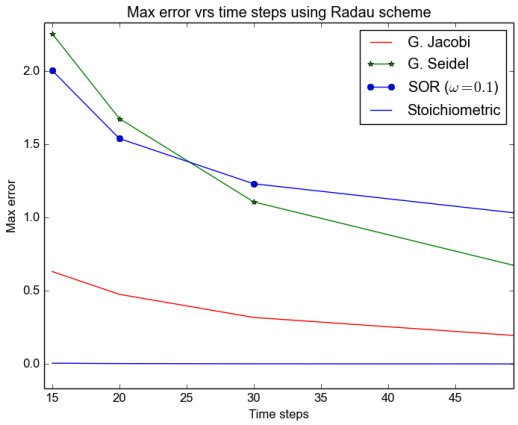

(d) Max. errors, using Radau scheme.

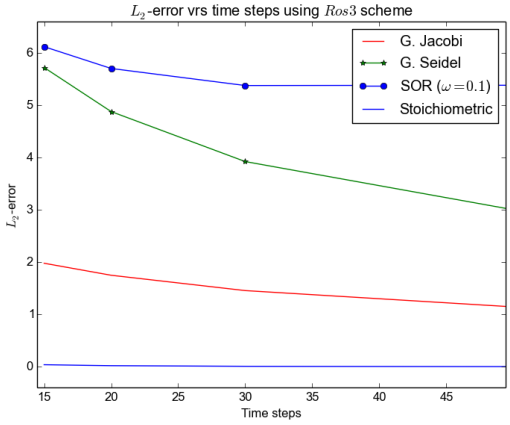

(e) L_2- errors, using *Rose3* scheme.

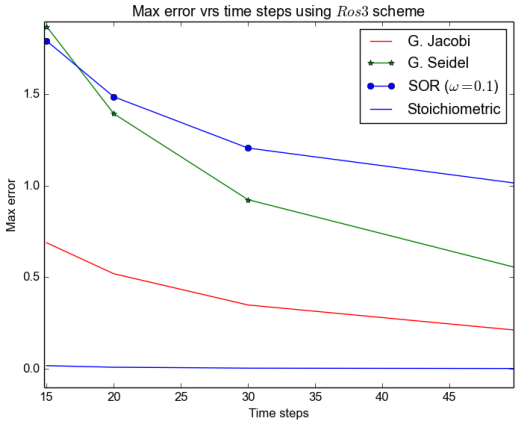

(f) Max. errors, using *Rose3* scheme.

Figure 4: Errors (max and L_2) of the numerical schemes, measured across decoupled models and time steps.

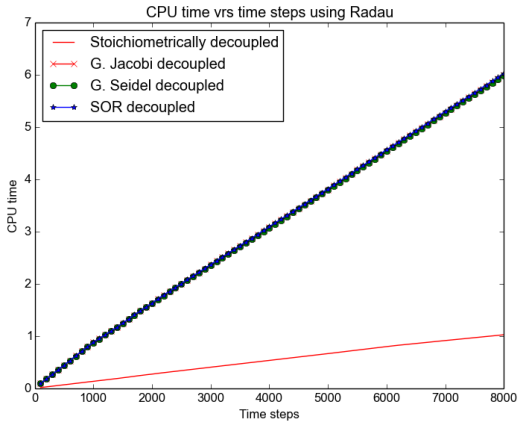

(a) CPU time using Radau scheme.

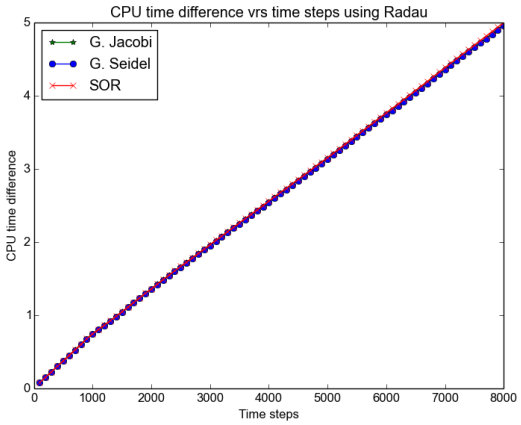

(b) CPU time difference using Radau.

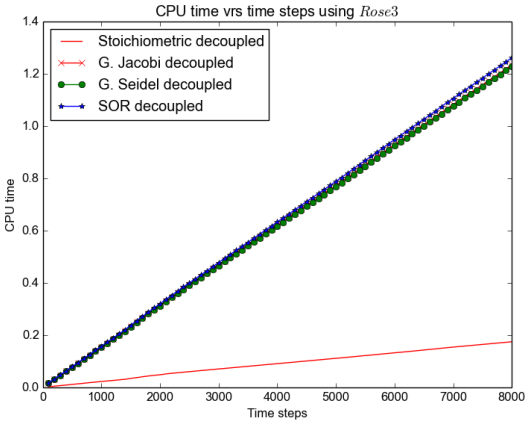

(c) CPU time using *Rose*3 scheme.

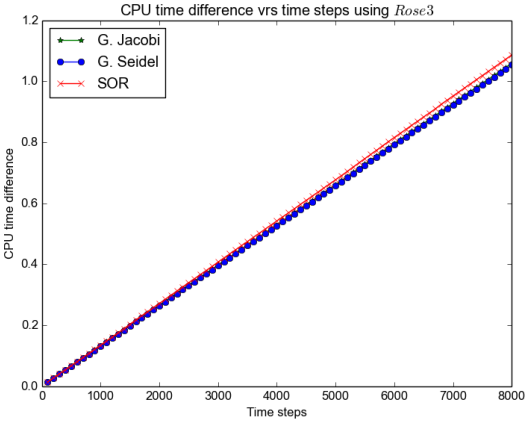

(d) CPU time difference using *Rose*3.

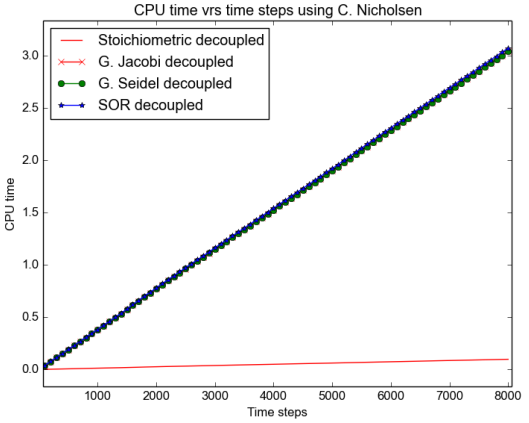

(e) CPU time using Crank-Nicholson scheme.

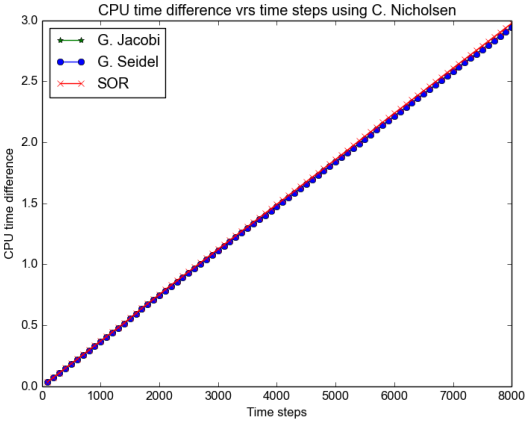

(f) CPU time difference using Crank-Nicholson.

Figure 5: CPU time and CPU time differences for *Gauss-Jacobi, Gauss-Seidel and SOR,* using *Radau,* Rose3 *and Crank-Nicholson*, measured across time steps (in the calcite model).

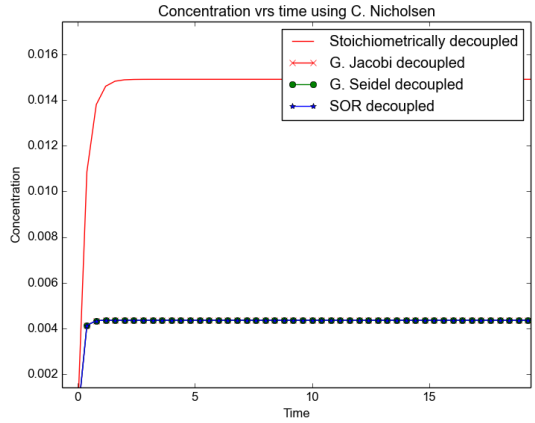

(a) Crank-Nicholson/50 time steps.

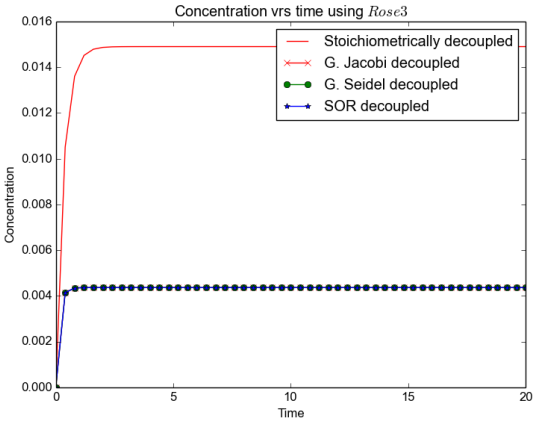

(b) *Rose3*/50 time steps.

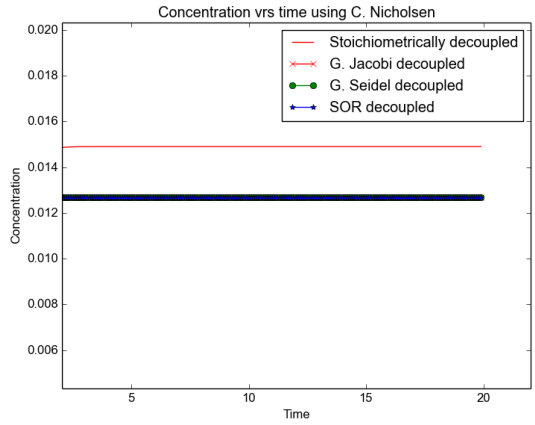

(c) Crank-Nicholson/200 time steps.

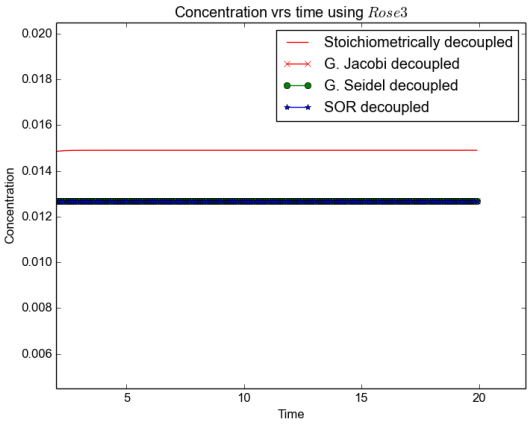

(d) *Rose3*/200 time steps.

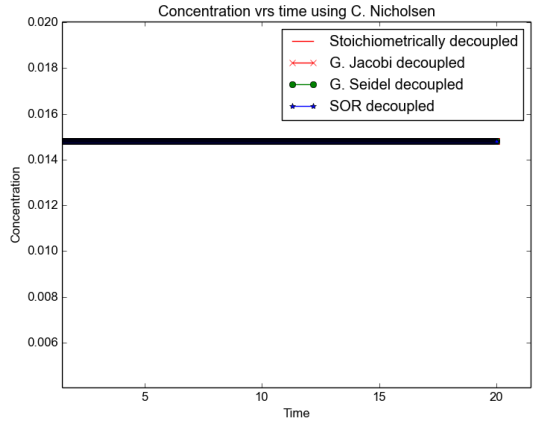

(e) Crank-Nicholson/8000 time steps.

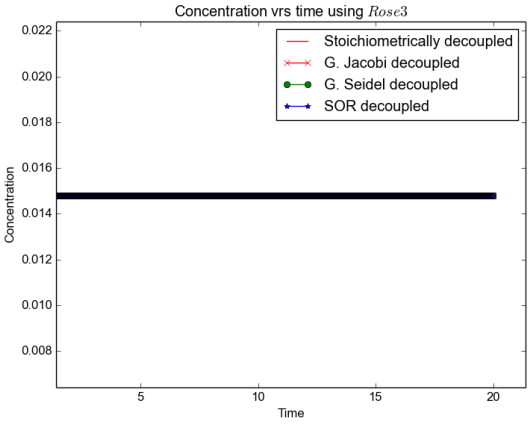

(f) *Rose3*/8000 time steps.

Figure 6: Hydrogen profiles in the *Gauss-Jacobi, Gauss-Seidel and SOR models* using Rose3 *and Crank-Nicholson*, measured across time steps (in the Pyrite model).

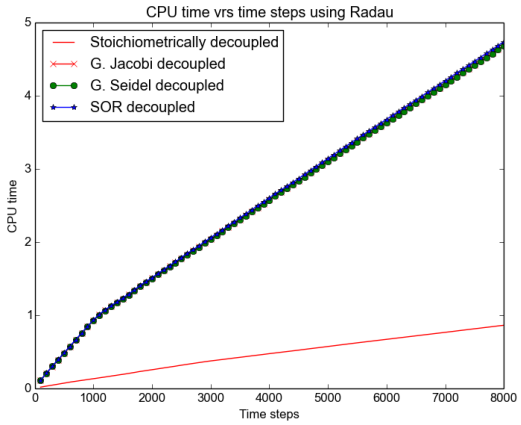

(a) CPU time using Radau scheme.

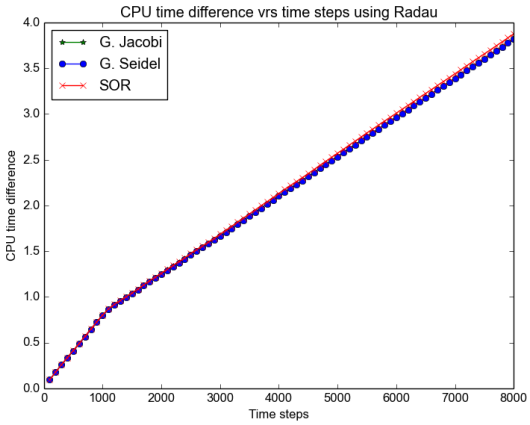

(b) CPU time difference using Radau scheme.

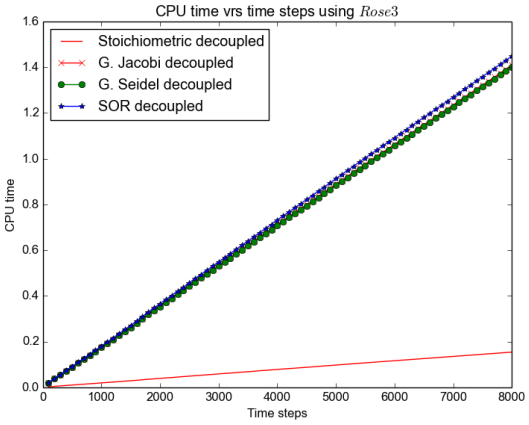

(c) CPU time using *Rose3* scheme.

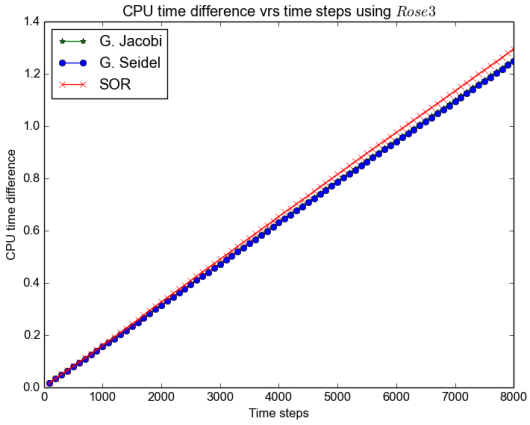

(d) CPU time difference using *Rose3* scheme.

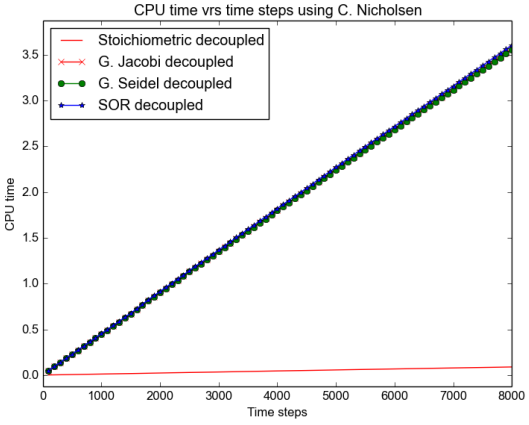

(e) CPU time using Crank-Nicholson scheme.

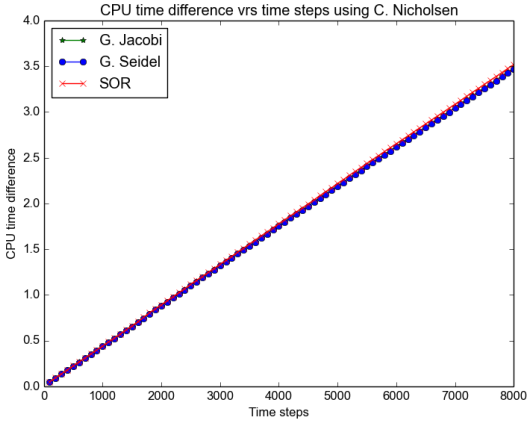

(f) CPU time difference using Crank-Nicholson scheme.

Figure 7: CPU time for the *Gauss-Jacobi, Gauss-Seidel and SOR* methods, using *Radau,* Rose3 *and Crank-Nicholson* schemes, measured across time steps in both calcite and pyrite models.

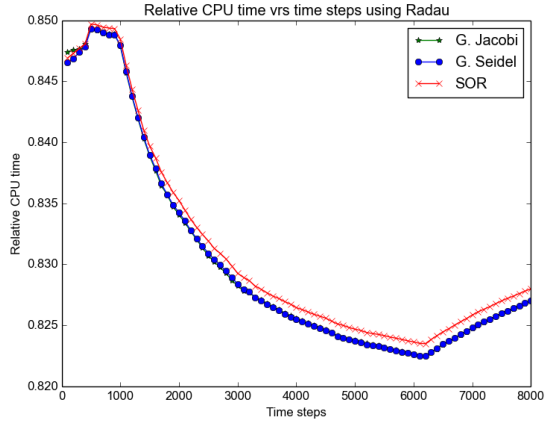

(a) Relative CPU time/Radau/Calcite model.

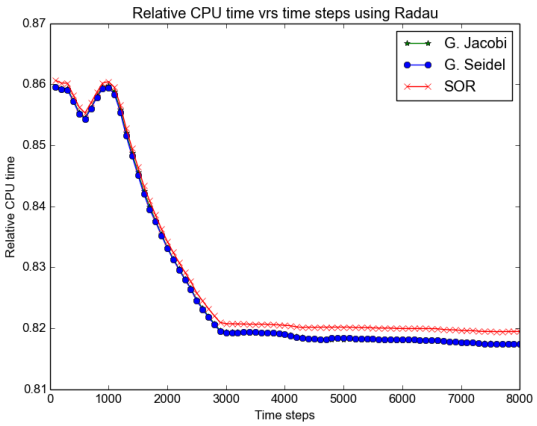

(b) Relative CPU time/Radau/Pyrite model.

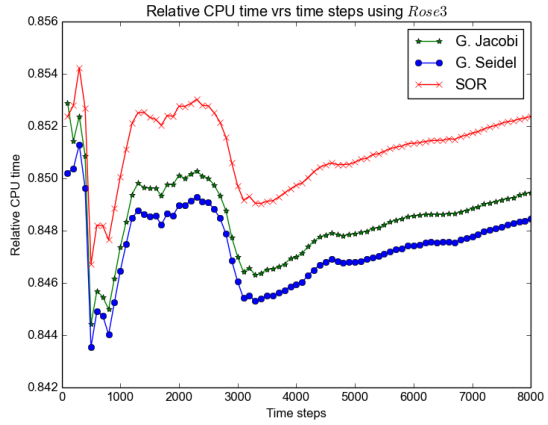

(c) Relative CPU time/*Rose3*/Calcite model.

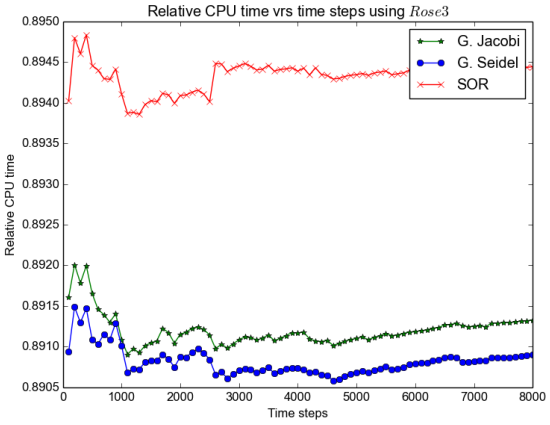

(d) Relative CPU time/*Rose3*/Pyrite model

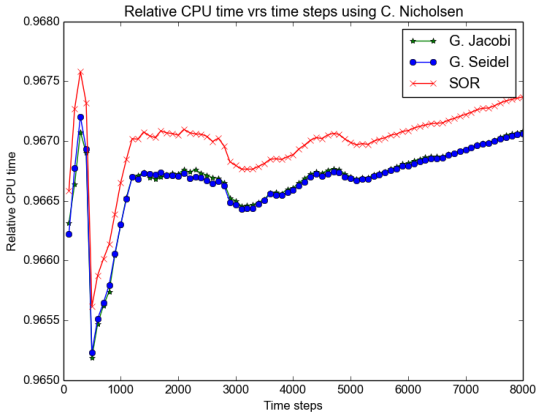

(e) Relative CPU time/Crank-Nicholson/Calcite.

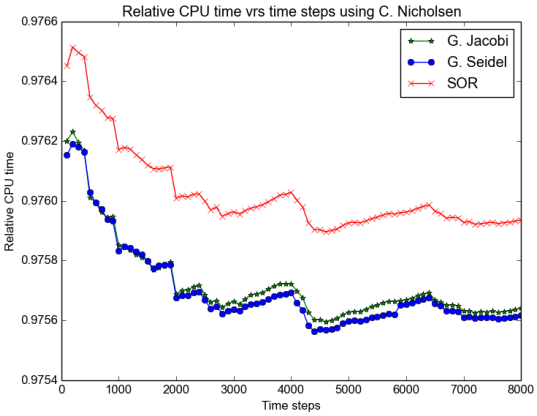

(f) Relative CPU time/Crank-Nicholson/Pyrite model.

Figure 8: Relative CPU time for *Gauss-Jacobi, Gauss-Seidel and SOR,* using *Radau,* Rose3 *and Crank-Nicholson* schemes, measured across time steps in both calcite and pyrite models.